

Towards a multi-platform assimilative system for North Sea biogeochemistry

Jozef Skákala^{1,2}, David Ford³, Jorn Bruggeman¹, Tom Hull^{4,5}, Jan Kaiser⁵, Robert R. King³, Benjamin Loveday¹, Matthew R. Palmer⁶, Tim Smyth¹, Charlotte A. J. Williams⁶ and Stefano Ciavatta^{1,2}

¹Plymouth Marine Laboratory, The Hoe, Plymouth, PL1 3DH United Kingdom.

²National Centre for Earth Observation, Plymouth, PL1 3DH, UK.

³Met Office, FitzRoy Road, Exeter, EX1 3PB UK.

⁴Centre for Environment, Fisheries and Aquaculture Science, Lowestoft, NR33 0HT UK.

⁵Centre for Ocean and Atmospheric Sciences, University of East Anglia, Norwich, NR4 7TJ, UK.

⁶National Oceanography Centre, Joseph Proudman Building, 6 Brownlow Street, Liverpool, L3 5DA UK.

Key Points:

- We successfully developed a multi-platform assimilative system for biogeochemistry in the North Sea.
- We tested the impact of the different assimilative system components on the ecosystem reanalysis.
- The multi-platform assimilation will become an essential part of future operational research.

Corresponding author: Jozef Skákala, jos@pm1.ac.uk

This article has been accepted for publication and undergone full peer review but has not been through the copyediting, typesetting, pagination and proofreading process, which may lead to differences between this version and the [Version of Record](#). Please cite this article as [doi: 10.1029/2020JC016649](https://doi.org/10.1029/2020JC016649).

This article is protected by copyright. All rights reserved.

Abstract

Oceanography has entered an era of new observing platforms, such as biogeochemical Argo floats and gliders, some of which will provide three-dimensional maps of essential ecosystem variables on the North-West European (NWE) Shelf. In a foreseeable future operational centres will use multi-platform assimilation to integrate those valuable data into ecosystem reanalyses and forecast systems. Here we address some important questions related to glider biogeochemical data assimilation and introduce multi-platform data assimilation in a (pre)operational model of the NWE Shelf-sea ecosystem. We test the impact of the different multi-platform system components (glider vs satellite, physical vs biogeochemical) on the simulated biogeochemical variables. To characterize the model performance we focus on the period around the phytoplankton spring bloom, since the bloom is a major ecosystem driver on the NWE Shelf. We found that the timing and magnitude of the phytoplankton bloom is insensitive to the physical data assimilation, which is explained in the study. To correct the simulated phytoplankton bloom one needs to assimilate chlorophyll observations from glider or satellite Ocean Color (OC) into the model. Although outperformed by the glider chlorophyll assimilation, we show that OC assimilation has mostly desirable impact on the sub-surface chlorophyll. Since the OC assimilation updates chlorophyll only in the mixed layer, the impact on the sub-surface chlorophyll is the result of the model dynamical response to the assimilation. We demonstrate that the multi-platform assimilation combines the advantages of its components and always performs comparably to its best performing component.

Plain Language Summary

North-West European (NWE) Shelf is a region of major importance for both European economy and climate. Observational oceanography has entered an important era of new observing biogeochemical platforms, such as Biogeochemical Argos and gliders. Gliders are being currently deployed to measure three-dimensional distributions of some essential biogeochemical variables on the NWE Shelf. This work establishes a multi-platform assimilative system on the NWE Shelf which will be used to combine multiple different types of observing platforms (e.g. satellite, gliders) with our up-to-date models in order to optimize our estimate and forecast of the NWE Shelf ecosystem state. We provide an understanding for how the different components of the system interact. We demonstrate that the assimilative system is skilled to combine physical data with satellite and glider data for chlorophyll, as well as the glider data for oxygen. The work establishes the foundations of a system that is planned to be used in the future operational oceanography on the NWE Shelf.

1 Introduction

Understanding the state and the future of shelf-sea ecosystems is essential from the point of view of economy, conservation and the global carbon cycle (*Pauly et al. (2002); Borges et al. (2006); Friedlingstein et al. (2006); Jahnke (2010)*). Reanalyses provide our best estimate of the ocean state by optimally combining the state-of-the-art knowledge from models with the most up-to-date observations. In marine biogeochemistry the prevailing approach is to assimilate satellite products into models, either for Ocean Color (OC) derived total chlorophyll (e.g. *Ishizaka (1990); Carmillet et al. (2001); Natvik and Evensen (2003); Hoteit et al. (2005); Triantafyllou et al. (2007); Nerger and Gregg (2007,0); Gregg (2008); Fontana et al. (2010); Ford et al. (2012); Ciavatta et al. (2011,0); Kalarni et al. (2016); Ford and Barciela (2017); Pradhan et al. (2019)*), Phytoplankton Functional Type (PFT)-specific chlorophyll (*Ciavatta et al. (2018,0); Skákala et al. (2018,0)*), or surface radiances (*Shulman et al. (2013); Ciavatta et al. (2014); Jones et al. (2016); Gregg and Rousseaux (2017); Skákala et al. (2020)*). Additionally a number of studies have assimilated biogeochemical data from in situ measurements, either using single-location

69 profiles (e.g. *Allen et al. (2003)*; *Hoteit et al. (2003)*; *Torres et al. (2006)*; *Lenartz et al.*
70 *(2007)*), or using surface data from ships, floats and buoys (e.g. *Anderson et al. (2000)*;
71 *Cossarini et al. (2009)*; *Song et al. (2016)*). The typical disadvantage of the tradition-
72 ally assimilated biogeochemical data-sets is that they are either constrained to the ocean
73 surface (e.g. in the case of satellite data), or they are typically limited to a single loca-
74 tion (in the case of vertically-measured data). Assimilating such data into the model has
75 either only local impact, or its impact on biogeochemical fields is typically constrained
76 to the upper oceanic layer, with uncertain impact on the vertical profiles of biomass, or
77 nutrients.

78 However, the situation on the data-front is rapidly changing, with new programmes
79 (e.g. AtlantOS, *Visbeck et al. (2015)*) aiming at revolutionizing biogeochemical oceanog-
80 raphy with novel observing platforms covering large parts of the ocean both horizontally
81 and vertically, such as floats deployed in the Biogeochemical-Argo programme (e.g. *John-*
82 *son and Claustre (2016)*; *Johnson (2016)*; *Germineaud et al. (2019)*), and gliders with
83 optical and biogeochemical sensors (*Telszewski et al. (2018)*). Some of the Argo float oxy-
84 gen data were already assimilated to constrain the biogeochemistry in the Southern Ocean
85 (*Verdy and Mazloff (2017)*) and Argo-measured chlorophyll was assimilated to improve
86 phytoplankton dynamics in the Mediterranean Sea (*Cossarini et al. (2019)*). This new
87 observational activity quite understandably focuses on regions of high importance for fish-
88 eries, economy and climate, such as the North-West European (NWE) Shelf (e.g. *Legge*
89 *et al. (2020)*), where a number of gliders have been deployed as a part of the Alterna-
90 tive Framework to Assess Marine Ecosystem Functioning in Shelf Seas (AlterECO) pro-
91 gramme (<http://projects.noc.ac.uk/altereco/>). The rapid development of these new au-
92 tonomous observation systems opens up an entirely new range of possibilities on how to
93 optimally integrate multi-platform observing networks with our present oceanographic
94 models (*Lellouche et al. (2013)*; *Bell et al. (2015)*). The observational work on the NWE
95 Shelf from the AlterECO project is coupled to a sister programme, the CAMPUS (Com-
96 bining Autonomous observations and Models for Predicting and Understanding Shelf seas,
97 <https://www.campus-marine.org/>) project, aiming to consistently combine the different
98 sources of information, such as gliders, satellite OC data and models, in order to improve
99 our capability to understand, represent and forecast the NWE Shelf biogeochemistry (e.g.
100 spring bloom, carbon and nutrient cycle, oxygen depletion events). Future plans, based
101 on CAMPUS and in line with the European Copernicus Marine Environment Monitor-
102 ing Service (CMEMS), are to have a multi-platform assimilative system on the NWE Shelf,
103 where the autonomous vehicles will navigate to specific locations using a combination
104 of Artificial Intelligence (AI) and model forecast, to observe important processes such
105 as the onset of the phytoplankton bloom, or hypoxic events.

106 Trying to establish glider data assimilation as part of such a multi-platform assim-
107 ilative system often leads to two non-trivial problems: a) how to consistently combine
108 high resolution glider data with much coarser model resolution, b) how to achieve rea-
109 sonable consistency between the assimilation-corrected variables and the coupled physical-
110 biogeochemical model dynamics. The problem of dynamical consistency needs special
111 mention, since both physical and biogeochemical fields have typically much larger gra-
112 dients in the vertical than in the horizontal dimension. The vertical correlation length
113 scales have large spatio-temporal variability and model dynamics can be quite sensitive
114 to spurious vertical gradients (*Doney (1999)*; *Oschlies and Garçon (1999)*; *Doney et al.*
115 *(2004)*). Such model sensitivity is often noticed when physical data (such as sea surface
116 height, or temperature and salinity) are assimilated into the model, as the spurious ver-
117 tical mixing introduced by such assimilation is known to often degrade the skill of the
118 biogeochemical model (e.g. *Berline et al. (2007)*; *While et al. (2010)*; *El Moussaoui et al.*
119 *(2011)*; *Holt et al. (2014)*; *Raghukumar et al. (2015)*; *Park et al. (2018)*). However, sim-
120 ilar issues can be easily overlooked when we assimilate surface biogeochemical data (ex-
121 cept extreme regions with substantial small-scale horizontal variability, such as the Gulf
122 Stream, *Anderson et al. (2000)*), since the biogeochemical fields have smaller gradients

123 in the horizontal direction than in the vertical, which means they are more dynamically
124 stable in the horizontal than in the vertical direction. For the gliders, it is of vital in-
125 terest to understand the potentially complex interaction between the physical and the
126 biogeochemical data assimilation, or the interplay between the different biogeochemical
127 variables updated by the assimilative system.

128 In this study we extend the operational assimilative system on the NWE Shelf to
129 successfully produce a multi-platform reanalysis including both physical (satellite sea sur-
130 face temperature, temperature and salinity from in situ platforms and an AlterEco glider)
131 and biogeochemical (total chlorophyll *a* and oxygen from an AlterECO glider, and chloro-
132 phyll *a* from a satellite OC product) variables. The main focus of the paper is to assess
133 the impact of the different multi-platform assimilative system components (satellite vs
134 glider, physical vs biogeochemical) on the simulated ecosystem processes in relation to
135 the phytoplankton spring bloom. Being able to estimate the impact of the different sys-
136 tem components is important, since it indicates what the assimilation impact will be on
137 the simulated biogeochemistry in regions where only a specific type of data (e.g. satel-
138 lite OC, physical variables) is available. The focus on the processes around the spring
139 bloom is a natural choice due to a) the availability of high quality chlorophyll glider data,
140 and b) because the spring bloom is a key driver of the ecosystem dynamics on the NWE
141 Shelf (*Lutz et al. (2007); Henson et al. (2009)*). The results of this study should form
142 a basis for an integrated multi-platform assimilative system, that will optimize the avail-
143 able information from observations and models in order to improve our understanding
144 of the NWE Shelf biogeochemistry. The assimilated biogeochemical glider variables were
145 selected based on the data availability, but both chlorophyll and oxygen are expected
146 to play an important role in the future multi-platform operational assimilation: chloro-
147 phyll is a proxy for phytoplankton biomass, which forms the base of the marine food web,
148 while oxygen needs to be monitored and forecast in order to identify oxygen depletion
149 events (i.e. hypoxia, *Vaquar-Sunyer and Duarte (2008)*), which can have disastrous im-
150 pacts on marine life.

151 2 Methods

152 The paper uses a hindcast version of the operational modelling system for the NWE
153 Shelf run by the Met Office in the framework of the CMEMS, i.e. the physical model Nu-
154 cleus for European Modelling of the Ocean (NEMO, *Madec et al. (2015)*) coupled through
155 the Framework for Aquatic Biogeochemical Models (FABM, *Bruggeman and Bolding (2014)*)
156 with the biogeochemical model European Regional Seas Ecosystem Model (ERSEM, *Baretta*
157 *et al. (1995); Blackford (1997); Butenschön et al. (2016)*). We used measurements from
158 an AlterEco glider that operated in the central North Sea between May-August 2018 pro-
159 viding data for temperature, salinity, chlorophyll (derived from fluorescence) and oxy-
160 gen concentrations. In multi-platform assimilation the glider data were complemented
161 with the Ocean Colour-Climate Change Initiative (OC-CCI) satellite product of the Eu-
162 ropean Space Agency (ESA) for total chlorophyll (version 3.1, *Sathyendranath et al. (2019)*),
163 Sea Surface Temperature (SST) data from the GCOM-W1/AMSR-2, NOAA/AVHRR,
164 MetOp/AVHRR, MSG/SEVIRI, Sentinel-3/SLSTR, and Suomi-NPP/VIIRS satellite
165 products, and the temperature and salinity in situ data from the EN4 dataset (*Good et al.*
166 *(2013)*), which includes profiles from Argo floats, fixed moored arrays, XBTs, CTDs, glid-
167 ers, and marine mammals. The physical and biogeochemical data were assimilated on
168 a daily basis into NEMO-FABM-ERSEM using NEMOVAR (the assimilative system used
169 operationally by the Met Office, *Mogensen et al. (2009,0); Waters et al. (2015); King et al.*
170 *(2018)*).

171 The model free simulation was run from 01/09/2017 until the end of the year 2018
172 and was initialized from a 2016-2018 run of a very similar model configuration presented
173 in *Skákala et al. (2020)*. The free run outputs have been analysed for the period of the
174 glider data availability (08/05-15/08, 2018). The assimilative runs used identical model

175 settings as the free run, only with the added assimilation components. The different as-
 176 similative runs compared in this study are (see also Table 1): a) physical data assimi-
 177 lation (satellite SST, temperature and salinity from EN4 data and the AlterEco glider),
 178 b) satellite OC total chlorophyll *a* assimilation, c) AlterEco glider chlorophyll *a* assimi-
 179 lation, d) AlterEco glider oxygen assimilation and e) multi-platform assimilation com-
 180 bining all the data from a)-d). Note that wherever we mention the assimilation of spec-
 181 ific data (e.g. glider chlorophyll) we mean a simulation where only those data have been
 182 assimilated (as opposed to multi-platform assimilation, which assimilates all the avail-
 183 able data). All the assimilative runs were started from the initial value conditions pro-
 184 duced by the free simulation for 08/05/2018.

185 **Table 1.** The observations assimilated in the different data assimilation (DA) experiments.
 186 The table uses some of the following abbreviations: temperature (T), salinity (S) and ‘EN4’
 187 means the EN4 in situ data-set.

Experiment	satellite SST	EN4 T&S	glider T&S	satellite OC	glider chl <i>a</i>	glider O ₂
physical DA	Yes	Yes	Yes	No	No	No
satellite OC DA	No	No	No	Yes	No	No
glider chl <i>a</i> DA	No	No	No	No	Yes	No
glider O ₂ DA	No	No	No	No	No	Yes
Multi-platform DA	Yes	Yes	Yes	Yes	Yes	Yes

188 2.1 The physical component: NEMO

189 The NEMO ocean physics component (OPA) is a finite difference, hydrostatic, prim-
 190 itive equation ocean general circulation model (*Madec et al. (2015)*). The NEMO con-
 191 figuration used in this study is similar to the one used by *Ford et al. (2017)*; *Skákala et al.*
 192 (2018), and almost identical to *Skákala et al. (2020)*: we use the CO6 NEMO version,
 193 based on NEMOv3.6, a development of the CO5 configuration explained in detail by *O’Dea*
 194 *et al. (2017)*. The model has 7 km spatial resolution on the Atlantic Margin Model (AMM7)
 195 domain using a terrain-following $z^*-\sigma$ coordinate system with 51 vertical levels (*Sid-*
 196 *dorn and Furner (2013)*). The lateral boundary conditions for physical variables at the
 197 Atlantic boundary were taken from the outputs of the Met Office operational 1/12° North
 198 Atlantic model (NATL12, *Storkey et al. (2010)*); the Baltic boundary values were derived
 199 from a reanalysis produced by the Danish Meteorological Institute for CMEMS. We use
 200 annually varying river discharge based on data from *Lenhart et al. (2010)*. The model
 201 was forced at the surface by atmospheric fluxes provided by an hourly and 31 km res-
 202 olution realisation (HRES) of the ERA5 data-set (<https://www.ecmwf.int/>).

203 2.2 The biogeochemical component: ERSEM

204 ERSEM (*Baretta et al. (1995)*; *Butenschön et al. (2016)*) is a lower trophic level
 205 ecosystem model for marine biogeochemistry, pelagic plankton, and benthic fauna (*Black-*
 206 *ford (1997)*). The model splits phytoplankton into four functional types largely based
 207 on their size (*Baretta et al. (1995)*): picophytoplankton, nanophytoplankton, diatoms
 208 and dinoflagellates. ERSEM uses variable stoichiometry for the simulated plankton groups
 209 (*Geider et al. (1997)*; *Baretta-Bekker et al. (1997)*) and each Phytoplankton Functional
 210 Type (PFT) biomass is represented in terms of chlorophyll, carbon, nitrogen and phos-
 211 phorus, with diatoms also represented by silicon. ERSEM predators are composed of three

zooplankton types (mesozooplankton, microzooplankton and heterotrophic nanoflagellates), with organic material being decomposed by one functional type of heterotrophic bacteria (*Butenschön et al. (2016)*). The ERSEM inorganic component consists of nutrients (nitrate, phosphate, silicate, ammonium and carbon) and dissolved oxygen. The carbonate system is also included in the model (*Artioli et al. (2012)*).

We used in this study a similar ERSEM configuration to *Skákala et al. (2020)*, but unlike *Skákala et al. (2020)* we implemented an updated ERSEM version (v20.10), with a notable upgrade to the benthic code. The ERSEM parametrization is identical to the one described in *Butenschön et al. (2016)*. The Atlantic boundary values for nitrate, phosphate, silicate and oxygen were taken from World Ocean Atlas (*Garcia et al. (2013)*) and dissolved inorganic carbon from the GLODAP gridded dataset (*Key et al. (2015)*; *Lauvset et al. (2016)*), while plankton and detritus variables were set to have zero fluxes at the Atlantic boundary. The ERSEM irradiance was calculated using a new bio-optical module implemented in the NEMO-FABM-ERSEM AMM7 configuration by *Skákala et al. (2020)*. The bio-optical module resolves light spectrally and distinguishes between downwelling direct and diffuse streams. The module is forced by ERA5 atmospheric inputs (<https://www.ecmwf.int/>) for total vertically integrated ozone, water vapour, cloud cover, cloud liquid water and sea-level air pressure, as well as by a satellite product for aerosol optical thickness (MODerate resolution Imaging Spectroradiometer, MODIS, <https://modis.gsfc.nasa.gov/data/dataproduct>).

2.3 The assimilative system: NEMOVAR

NEMOVAR is a variational Data Assimilation (DA) system (*Mogensen et al. (2009,0)*; *Waters et al. (2015)*) used for operational ocean DA at the Met Office. Via the assimilation of satellite OC derived (total, or PFT) chlorophyll concentrations, NEMOVAR has been demonstrated as being highly successful in improving the phytoplankton community structure (PFT chlorophyll assimilation), phytoplankton seasonal cycle and the timing and magnitude of the spring bloom (*Skákala et al. (2018,0)*). There are also indications that satellite OC assimilation can improve the carbon cycle (*Skákala et al. (2018,0)*). When it comes to the non-assimilated variables, satellite OC reanalysis typically has a comparable skill to the free run (*Skákala et al. (2018,0)*). The satellite OC chlorophyll assimilation using NEMOVAR on the NWE Shelf has been thoroughly validated on bi-decadal time-scales (*Kay et al. (2019)*), showing a good overall skill and no spurious trends in biogeochemical tracer concentrations.

In this study the observations are assimilated on a daily basis. The model is first run for the day and background values are calculated in observation space by interpolating the model fields to the observation locations at the nearest model time step (300 seconds) to the observation time, an approach known as First Guess at Appropriate Time (FGAT). NEMOVAR is then run, calculating a set of increments for each updated variable on the model grid. After the assimilation step the model is re-run with the increments applied to the model variables gradually at each model time-step using incremental analysis updates (IAU, *Bloom et al. (1996)*). For the physical variables the increments are calculated for temperature, salinity, sea surface height and the horizontal velocity components, by accounting for their correlations by transforming those variables through a set of linear balancing equations into an independent set of variables that is assimilated separately. For biogeochemical variables, the increments are initially calculated for the observed variable. For total chlorophyll the assimilation is applied in log-space, since chlorophyll is typically log-normally distributed (*Campbell (1995)*). After calculating the total chlorophyll increments, we use a balancing module to split those increments into the model state variables. The applied scheme (*Skákala et al. (2018,0)*) redistributes total chlorophyll increments into the 4 ERSEM PFTs based on background PFT-to-total chlorophyll ratios. The PFT chlorophyll is used to update the remaining PFT components (carbon, phosphorus, nitrogen for all PFTs, silicon for diatoms) following the back-

264 ground stoichiometric ratios. In the case of oxygen assimilation the only updated vari-
 265 able is the simulated oxygen concentration. There were attempts to extend the currently
 266 applied balancing scheme to other ERSEM variables (e.g nutrients), but so-far this pro-
 267 duced sub-optimal results degrading the biogeochemical model skill (see discussion in
 268 *Skákala et al. (2018)*). Any combined physical-biogeochemical assimilation in NEMOVAR
 269 is weakly coupled, which means that the physical and the biogeochemical variables are
 270 assimilated separately, with physical assimilation impacting biogeochemistry only through
 271 the model dynamics, and no feedback from biogeochemistry to physics.

272 The multi-platform assimilation is based on the development from *Waters et al.*
 273 (2015) extended to biogeochemical variables by *Ford (2020)*, i.e. the combined assim-
 274 ilation of satellite OC and glider chlorophyll data is performed by following a scheme pre-
 275 viously applied to temperature by *Waters et al. (2015)*. The satellite and in situ glider
 276 data are combined to calculate a single set of 3D increments, while allowing for differ-
 277 ent observation errors to be specified for the different data sources (for the details see
 278 *Waters et al. (2015); Ford (2020)*). Since each of the physical data, chlorophyll and oxy-
 279 gen assimilation provides increments for different variables, the multi-platform assim-
 280 ilation simply aggregates the increments from the physical, chlorophyll and oxygen as-
 281 similative components.

282 The background covariances are represented as a product of background variances
 283 and a diffusion operator (*Mirouze and Weaver (2010); King et al. (2018)*). Within the
 284 diffusion operator, the same length-scales are set for all the assimilated (physical, bio-
 285 geochemical) variables. The horizontal correlation length-scales are specified a-priori, and
 286 are based on two different length scales, a longer 100 km correlation scale and a shorter
 287 length-scale based on the first baroclinic Rossby radius of deformation (*King et al. (2018)*).
 288 The vertical length-scales use the scheme from *Waters et al. (2015); King et al. (2018);*
 289 *Ford (2020)*, where NEMOVAR calculates directly the set of 3D increments (we call this
 290 scheme a “3D variant”) using flow-dependent vertical length-scales (ℓ), which are the fol-
 291 lowing function of depth (d):

$$\begin{aligned} \ell(d) &= \frac{d_{\text{ml}}}{2} - \left(\frac{1}{2} - \frac{2G(d_{\text{ml}})}{d_{\text{ml}}} \right) \cdot d, & 0 \leq d \leq d_{\text{ml}}, \\ \ell(d) &= 2G(d), & d > d_{\text{ml}}, \end{aligned} \quad (1)$$

292 where d_{ml} is the mixed layer depth (MLD) and $G(d)$ is the vertical grid spacing as a func-
 293 tion of depth. Equation 1 means the surface length-scale is equal to half of the MLD,
 294 the length scale decreases linearly with depth until the MLD, while beneath MLD the
 295 length-scales are two times the local vertical grid resolution. Such vertical correlation
 296 length-scales are designed to minimise any spurious mixing of surface increments beneath
 297 the mixed layer (*King et al. (2018)*). It should be noted that satellite OC data assim-
 298 ilation in some previous studies (e.g. *Skákala et al. (2018,0)*) used a “2D variant”, where
 299 surface chlorophyll increments were applied throughout the mixed layer. Both 2D and
 300 3D variants were tested in this study and we have found that they produced almost iden-
 301 tical results (not shown here). In this study we will present the outputs of the 3D vari-
 302 ant, but these are representative of both methods.

303 NEMOVAR has two important drawbacks: (i) the background errors (square-root
 304 of background variances) have to be specified mostly a priori and those do not always
 305 capture how the reanalysis approximates the true state, (ii) it does not account for the
 306 observational error correlations. Both (i) and (ii) tend to artificially increase the impact
 307 of the assimilated observations (especially when there is high density of observations)
 308 and likely contribute to the fact that biogeochemical reanalyses on the NWE Shelf are
 309 relatively insensitive to the precise value of the background-to-observational error ratio
 310 (e.g. *Skákala et al. (2018)*). Then, provided that the reanalysis state is sufficiently in-
 311 ternally consistent, NEMOVAR reanalyses on the NWE Shelf tend to converge for a wide
 312 interval of background-to-observational error ratios towards the assimilated observations

313 (*Skákala et al. (2018,0)*). Improvements could be achieved by using hybrid methods (e.g.
 314 background errors calculated as a weighted combination of the parameterised compo-
 315 nent and a flow-dependent component calculated from an ensemble), or flow-dependent
 316 iterative methods based on error diagnostics, such as the scheme of *Hollingsworth and*
 317 *Lönnberg (1986)*; *Andersson (2003)*; *Desroziers et al. (2005)* (e.g. *Mattern et al. (2018)*;
 318 *Cossarini et al. (2019)*). For physical assimilation (*King et al. (2018)*) the background
 319 errors were estimated using the innovation method of *Hollingsworth and Lönnberg (1986)*
 320 applied to innovations from an existing reanalysis by *O’Dea et al. (2017)*, with background
 321 errors between 1-3.5 times larger than the observational errors (Table 2). For biogeochem-
 322 ical assimilation the background errors, $\Sigma\{Q_{\text{bkg}}\}$, were estimated from the observational-
 323 to-free run differences and observational errors, $\Sigma\{Q_{\text{o}}\}$, (Q_{bkg} , Q_{m} and Q_{o} stand sub-
 324 sequently for the background, model free run and observed concentrations), along the
 325 scheme of *Skákala et al. (2020)*:

$$\Sigma\{Q_{\text{bkg}}\} = \sqrt{[(Q_{\text{m}} - Q_{\text{o}})^2] - \Sigma\{Q_{\text{o}}\}^2}, \quad (2)$$

326 which assumes that for a suitable spatio-temporal binning the model and observational
 327 errors are uncorrelated (*Skákala et al. (2020)*). In the case of the glider data the total
 328 observational errors (including representation error) were estimated from the difference
 329 between variances of the observations, $V\{Q_{\text{o}}\}$, and the variances of the true state, $V\{Q_{\text{t}}\}$:

$$\Sigma\{Q_{\text{o}}\} = \sqrt{V\{Q_{\text{o}}\} - V\{Q_{\text{t}}\}}, \quad (3)$$

335 where the variances of the true state were estimated from the model outputs. This scheme
 336 assumes that the observations have zero bias and that (for the limited spatio-temporal
 337 range of glider data) the observational errors and the true state deviations from the mean
 338 are uncorrelated. After estimating the observational errors for gliders, one proceeds with
 339 the equation 2 to estimate the corresponding background errors. The methods based on
 340 equation 2 and equation 3 produced background and observational errors with compa-
 341 rable values, with background-to-observational error ratios on average between 0.77-2.3
 (see Table 2). For the two different chlorophyll observational products, the estimate of

330 **Table 2.** The Table shows parts of the multi-platform assimilative system with the list of
 331 the updated physical-biogeochemical variables and the mean values of the background-to-
 332 observational error ratio (B-O error ratio, with error understood as standard deviation). The
 333 physical variables are abbreviated as temperature (T), salinity (S), sea surface height (SSH) and
 334 horizontal velocity components (U,V).

component	updated variables	B-O error ratio
satellite OC chl <i>a</i>	PFT components	2.3
glider chl <i>a</i>	PFT components	1.4
glider O ₂	oxygen	0.77
satellite T	T,S,SSH,U,V	1.55
in situ T	T,S,SSH,U,V	1.04
in situ S	T,S,SSH,U,V	3.42

342 glider chlorophyll error (using equation 3) turned out to be on average 22% lower than
 343 the satellite OC chlorophyll error.
 344

2.4 Glider data

The study used data from a Slocum glider (Teledyne Webb Research, Falmouth, USA) named Cabot (Unit 345, National Oceanography Centre, Southampton) deployed during the AlterEco mission (deployment 454). The glider sampling transect was situated in the Central North Sea (see Figure 1), between May-August 2018, collecting data for temperature and salinity (Seabird SBE42 CTD), colored dissolved organic matter, particulate backscattering, chlorophyll *a* fluorescence (Wetlabs ECOpuck), and oxygen (Aanderaa AA4831 optode). After Quality Control (QC) the quenching-corrected chlorophyll (derived from fluorescence) and oxygen concentrations were available for slightly different periods: chlorophyll for 08/05 - 15/08, 2018 and oxygen for a shorter period of 08/05 - 30/06, 2018. The Cabot glider was chosen because it provided high-quality data, but the period of the glider mission was also of special interest for assimilation, since it marks a known discrepancy between the timing of the spring bloom in the model and observations, with the model biased towards a late bloom (see *Skákala et al. (2020)*). The QC glider outputs contained a substantial number of data-points ($2 \cdot 10^6$ for chlorophyll and $3 \cdot 10^5$ for oxygen) which were mapped to the model AMM7 grid (each observation to the nearest model grid point). The observations that were mapped on the same day into the same model grid point were then averaged into a single value. The grid-averaging of glider observations is a practice adopted in the physical DA to avoid assimilating many observations at higher resolution than the model can represent. However, our tests have shown that the impact of grid-averaging on the biogeochemical reanalysis was negligible. During each day the glider typically covered 3 model horizontal grid-cells and for each model horizontal location the glider scanned nearly the full vertical water column.

The glider data (publicly available from www.bodc.ac.uk) were processed by the National Oceanography Centre (NOC) AlterECO team using the GEOMAR glider toolbox for salinity and oxygen lag corrections (following *Bittig et al. (2014)*). The glider was fitted with a standard non-pumped SBE CT sensor, a WETLabs ECOpuck to measure chlorophyll fluorescence, and an Aanderaa 4330 oxygen optode. Oxygen data were corrected based on comparisons between Winkler samples and local crossings with the rest of the AlterEco glider fleet.

The fluorescence sensor on Cabot (454) was calibrated prior to deployment, and recovered data were converted to chlorophyll concentration from raw voltages using the manufacturer supplied calibration routine. The derived chlorophyll record was filtered such that negative values were set to zero. Multiple quenching corrections were tested, including: *Hemsley et al. (2015)*; *Swart et al. (2015)*; *Biermann et al. (2015)* and *Xing et al. (2012)*. The former three methods rely on the use of algal particle scattering to correct for quenching. However, these approaches proved unsatisfactory for use in case-2 waters (e.g. the North Sea). Consequently, the *Xing et al. (2012)* method was adopted. Under this approach the maximum value of chlorophyll concentration above the mixed layer depth (MLD) is extrapolated to the surface for daytime profiles. Night-time chlorophyll profiles are not corrected. MLD is calculated from glider CTD profiles according to the method of *Holte and Talley (2009)*.

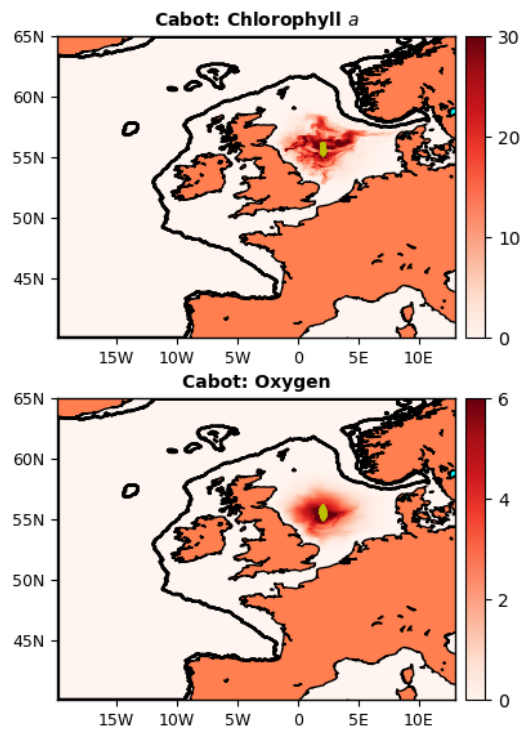
2.5 Used metrics (definitions)

The paper uses two metrics: a) model-to-observation bias (ΔQ_{mo}) defined as

$$\Delta Q_{mo} = \langle Q_m - Q_o \rangle, \quad (4)$$

where, as before, Q_m are the model free run and Q_o the observed concentrations (by the observations we will automatically mean the glider data), and b) Bias-Corrected Root Mean Square Difference (BC RMSD, $\Delta_{RD} Q_{mo}$) defined as

$$\Delta_{RD} Q_{mo} = \sqrt{\langle [Q_m - Q_o - \Delta Q_{mo}]^2 \rangle}. \quad (5)$$



368 **Figure 1.** The panels show the NEMO-FABM-ERSEM (AMM7) domain with the Cabot
 369 glider data locations (chlorophyll data locations for the full 08/05-15/08, 2018 mission, oxygen
 370 data for a shorter period of 08/05-29/06, 2018) marked by yellow dots, as well as glider horizontal
 371 area of impact on the reanalysis. The color scale in the two panels shows the weekly (23-29-th
 372 June 2018) mean percentage (%) difference between reanalysis and free run in the surface chloro-
 373 phyll (upper panel) and surface oxygen (bottom panel) concentrations, and reveals the horizontal
 374 extent of the glider’s impact on the assimilation. The percentage difference is calculated by di-
 375 viding the absolute value of the difference between reanalysis and the free run, with the free run.
 376 The black lines show the boundary of the NWE Shelf (≤ 200 m bathymetry).

401 The BC RMSD metric is applied in two different contexts: as a “spatial BC RMSD” and
402 a “temporal BC RMSD”.

403 In the case of spatial BC RMSD, we calculate for each day (t_d) the difference be-
404 tween the model and the observed daily mean, which we call model-to-observation daily
405 bias:

$$\Delta Q_{\text{mo}}(t_d) = \langle Q_{\text{m}}(t_d) - Q_{\text{o}}(t_d) \rangle, \quad (6)$$

406 where $Q_{\text{m}}(t_d)$ and $Q_{\text{o}}(t_d)$ are the model free run and the observation data from the day
407 t_d , and the model free run is taken only from the spatial locations visited by the glider
408 (about 150 model grid points per day). Then we calculate “daily BC RMSD”, $\Delta_{\text{RD}}Q_{\text{mo}}(t_d)$,
409 by applying equation 5 on each day using the model and the observation daily data, as
410 well as their daily biases:

$$\Delta_{\text{RD}}Q_{\text{mo}}(t_d) = \sqrt{\langle [Q_{\text{m}}(t_d) - Q_{\text{o}}(t_d) - \Delta Q_{\text{mo}}(t_d)]^2 \rangle}. \quad (7)$$

411 The spatial BC RMSD, $\Delta_{\text{RD}}^{\text{S}}Q_{\text{mo}}$, is then obtained as a time-average of the daily BC
412 RMSD, i.e. averaging $\Delta_{\text{RD}}Q_{\text{mo}}(t_d)$ through the glider data availability period (100 days
413 for chlorophyll and 53 days for oxygen):

$$\Delta_{\text{RD}}^{\text{S}}Q_{\text{mo}} = \langle \Delta_{\text{RD}}Q_{\text{mo}}(t_d) \rangle_{t_d}, \quad (8)$$

414 where $\langle \rangle_{t_d}$ means averaging through the interval of t_d values. Since the glider moves on
415 the model grid dominantly in the vertical dimension, the spatial BC RMSD mostly mea-
416 sures how well the model simulation represents the vertical profile of the glider obser-
417 vations.

418 The temporal BC RMSD, $\Delta_{\text{RD}}^{\text{T}}Q_{\text{mo}}$, is based on calculating a time-series, δ , of the
419 daily mean values (for both model, δ_{m} , and the observations, δ_{o}), averaged through the
420 spatial locations visited by the glider:

$$\delta_{\text{m}}(t_d) = \langle Q(t_d) \rangle, \quad \delta_{\text{o}}(t_d) = \langle Q_{\text{o}}(t_d) \rangle, \quad (9)$$

421 then applying equation 5 to those time-series, with bias understood as the model-to-observation
422 difference in the temporal mean of the time-series data:

$$\Delta_{\text{RD}}^{\text{T}}Q_{\text{mo}} = \sqrt{\langle [\delta_{\text{m}}(t_d) - \delta_{\text{o}}(t_d) - \langle \delta_{\text{m}}(t_d) - \delta_{\text{o}}(t_d) \rangle]^2 \rangle_{t_d}}. \quad (10)$$

423 The temporal BC RMSD is designed to capture how the model represents the observed
424 phytoplankton phenology.

425 It should be noted that the metrics discussed in this section are used to measure
426 “the skill” of the assimilative runs by comparing the simulation outputs to the assim-
427 ilated glider data, rather than to an independent validation data-set. There are two rea-
428 sons for this: firstly, to get sufficient validation data for the limited spatio-temporal re-
429 gion of this study is nearly impossible, however, most importantly, this study has no am-
430 bition to produce a skill-assessed reanalysis, its ambition is to test the impact of the as-
431 similative system components on the simulated variables. Since the NEMOVAR reanal-
432 yses tend to converge under optimal conditions to the assimilated observations (*Skákala*
433 *et al.* (2018,0)), the performance of the assimilative system can be measured by compar-
434 ing the model to the assimilated data.

435 3 Results and Discussion

436 The model free run shows a late and intense spring bloom, with a timing about 1
437 month later than the bloom observed in the satellite OC and in situ data (Figure 2 and
438 *Skákala et al.* (2020)). The late timing of the model bloom is most likely influenced by
439 the interplay between the model vertical mixing scheme and the simulated irradiance (see

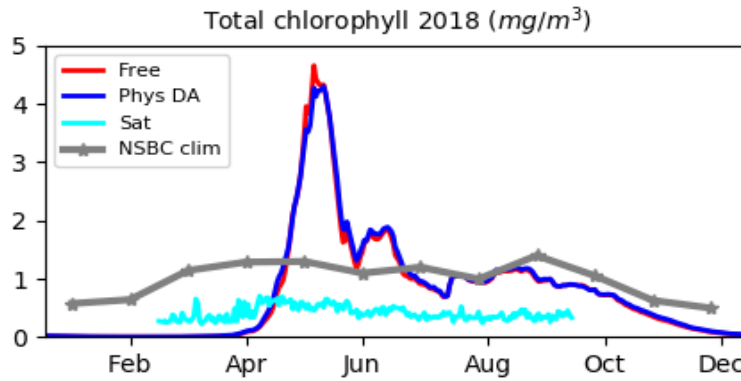
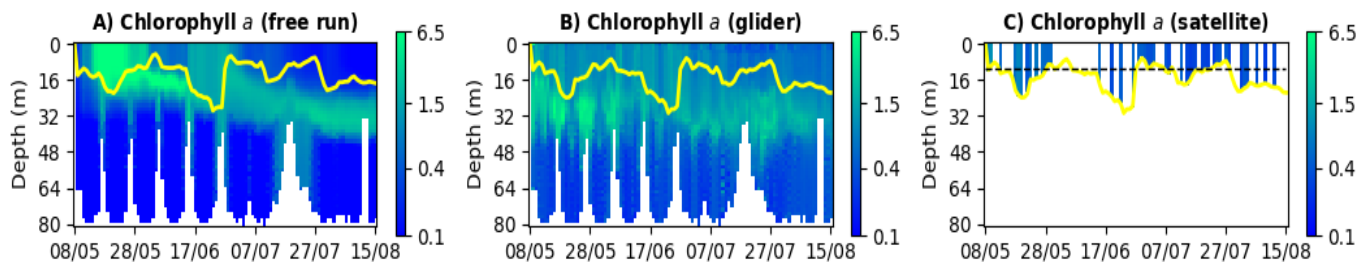


Figure 2. The mean daily surface chlorophyll concentrations averaged across the NWE Shelf for the year 2018. We compare a model free run used in this study with the physical data assimilation (the physical data assimilation started on 01/09 2017 from the model free run initial values), the satellite OC and the North Sea Biogeochemical Climatology (NSBC) in situ data set (*Hinrichs et al. (2017)*). The satellite OC chlorophyll values are masked for the October-February period when there is sparsity of data due to the extensive cloud cover and the low solar zenith angle. The model is shown to have an intense and late spring bloom: the observed bloom is much less pronounced than the bloom in the model and the timing of the observed bloom is around the early April, as opposed to the early-mid May bloom simulated by the model.

the discussion in *Skákala et al. (2020)*). The results from the study of *Skákala et al. (2020)* are confirmed by Figure 3, which shows the chlorophyll concentrations in the region measured by the glider between May and August 2018. When the assimilation starts in early May (Figure 3), the glider is in the post-bloom period showing some deep chlorophyll maxima, whereas the model free run has yet to see the onset of the bloom with chlorophyll concentrations predominantly in the mixed layer. Since the North Atlantic sees substantial seasonal patterns in primary productivity (e.g. *Henson et al. (2009)*), the late and intense model bloom has a large impact on the biogeochemical model skill (*Skákala et al. (2020)*).

The simulated surface chlorophyll on the NWE Shelf is typically corrected by the assimilation of OC satellite data (*Skákala et al. (2018,0)*) and the positive impact of satellite OC assimilation on the simulated NWE Shelf surface chlorophyll is shown in Figure 4:A-B. Around the glider locations, it is shown that both satellite OC and glider chlorophyll assimilation remove the late simulated bloom and improve the surface phytoplankton phenology (Figure 5:D,F, Figure 6:A-B). However, unlike the satellite OC component, the glider chlorophyll assimilation has a limited impact on the model domain (Figure 4:D). The horizontal spatial impact of glider assimilation varies with time (Figure 7A-B), but any substantial impact of glider assimilation on the simulated chlorophyll (on the level of $\geq 10\%$) is typically constrained to a 50 km radius around the glider location (Figure 7:A).

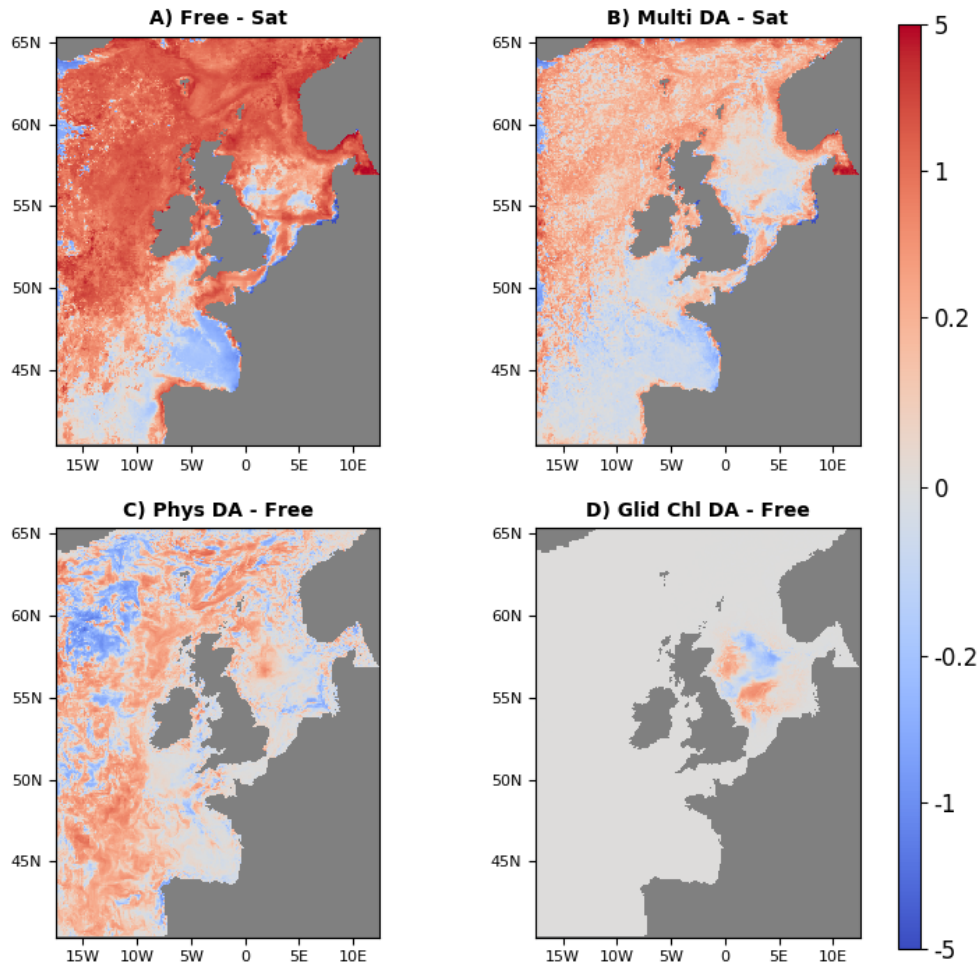
Since glider chlorophyll *a* data were assimilated across the whole water column, the glider chlorophyll assimilation is also able to substantially improve the sub-surface chlorophyll concentrations (Figure 5:F). The three skill metrics (bias, spatial and temporal BC RMSD) capturing how the simulated chlorophyll *a* matches with the glider observations were all substantially improved by the glider chlorophyll assimilation: the model bias was reduced by almost 50% (Table 3 and Figure 6:D), the spatial BC RMSD by 60% (Table 3) and the temporal BC RMSD by 70% (Table 3). Unlike glider chlorophyll assimilation, satellite OC assimilation updates chlorophyll concentrations only in the mixed



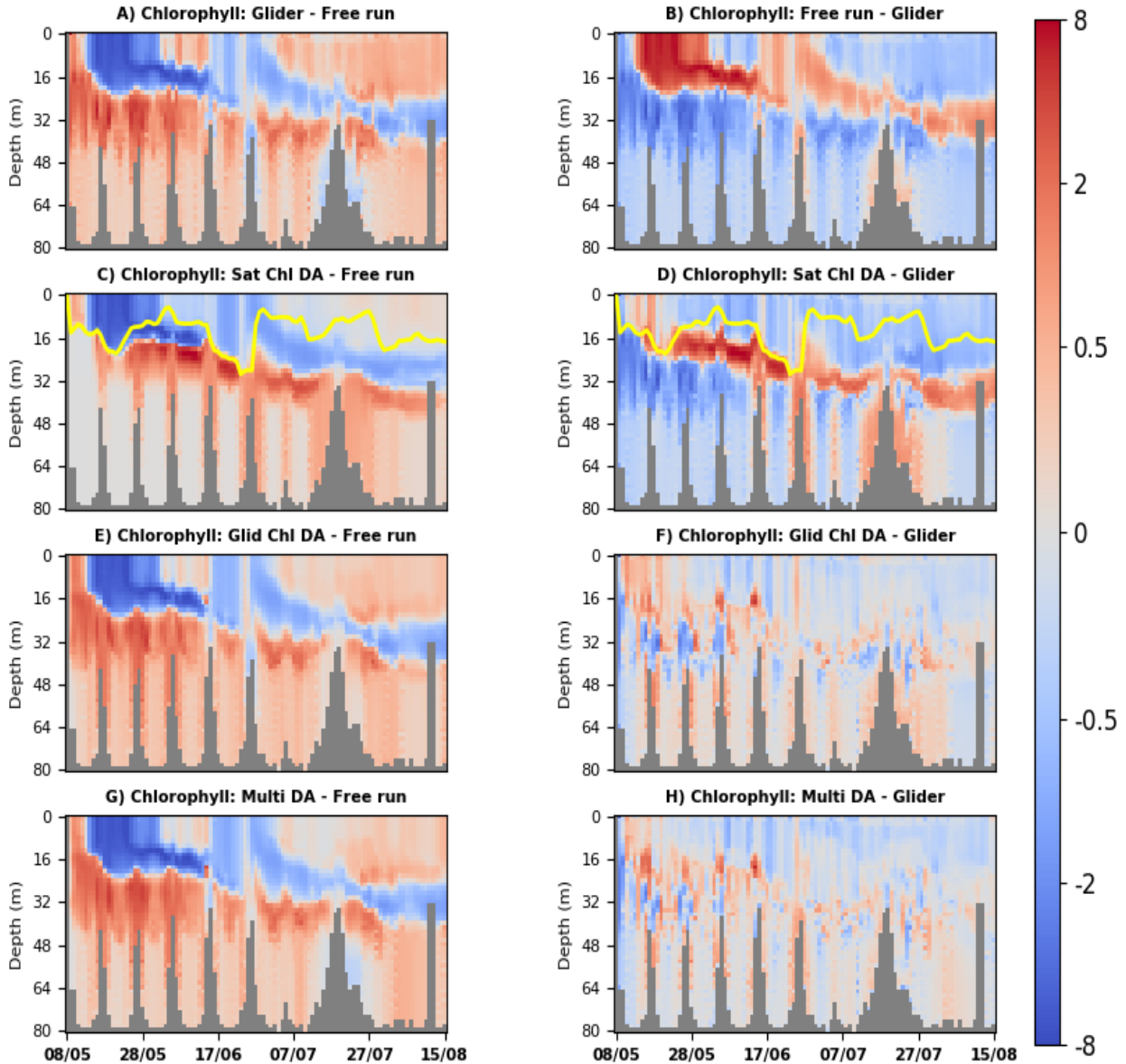
458 **Figure 3.** Hovmöller diagrams for the model free run and the observations. The left panel (A)
 459 shows the model free run outputs for total chlorophyll a (mg m^{-3}) horizontally averaged through
 460 the area covered by the glider during each day (the plot is depth vs time). The middle panel
 461 (B) shows the same for the glider-observed chlorophyll concentrations and the right panel (C)
 462 shows the satellite OC chlorophyll observations at the glider locations. The yellow lines mark the
 463 mixed layer depth of the model free run (left-hand panel) and of the physics-assimilative run (the
 464 middle and right-hand panels). The satellite observations are plotted in the mixed layer, with
 465 the dotted black line broadly corresponding to the average satellite optical depth (*Skákala et al.*
 466 (2020)). The several missing data in the right hand plot are due to the cloud cover. The missing
 467 data at the bottom of panels A-B are due to the varying bathymetry along the horizontal glider
 468 trajectory.

488 layer, but the model dynamics propagates the updates to chlorophyll beneath the mixed
 489 layer and gradually spreads the impact of assimilation across the whole water column
 490 (Figure 5:C). It is encouraging to see that the model dynamics acting on the satellite OC
 491 assimilation increments produces a qualitatively similar change to the sub-surface chloro-
 492 phyll as the glider assimilation (Figure 5:C and Figure 5:E). We propose a simple ex-
 493 planation based on chlorophyll dynamics: The satellite-only assimilative run removes the
 494 intense late model bloom in May, removing chlorophyll from the mixed layer and increas-
 495 ing the light penetrating into the water column. The increased irradiance combined with
 496 nutrient availability produces deep chlorophyll maxima around the pycnocline (Figure
 497 5:C). Furthermore, the removal of the late (mid-May) bloom in the satellite OC reanal-
 498 ysis means the assimilation also removes the gradually deepening chlorophyll maxima
 499 (the July-August period in Figure 3:B and Figure 4:C), as the nutrients become confined
 500 deeper in the water column. The satellite OC assimilation improves both temporal BC
 501 RMSD (by 55%, Table 3) and spatial BC RMSD (by 15%, Table 3). Although the im-
 502 provement of BC RMSD is in both cases outperformed by the glider chlorophyll assimi-
 503 lation, the substantial reduction of temporal BC RMSD by 55% in the satellite OC rean-
 504 alysis is non-trivial, and it is only possible due to (i) a relative consistency between
 505 the satellite OC data and the glider surface measurements (Figure 3, Figure 6:A-B), and
 506 (ii) a realistic update to sub-surface chlorophyll driven by the model dynamics.

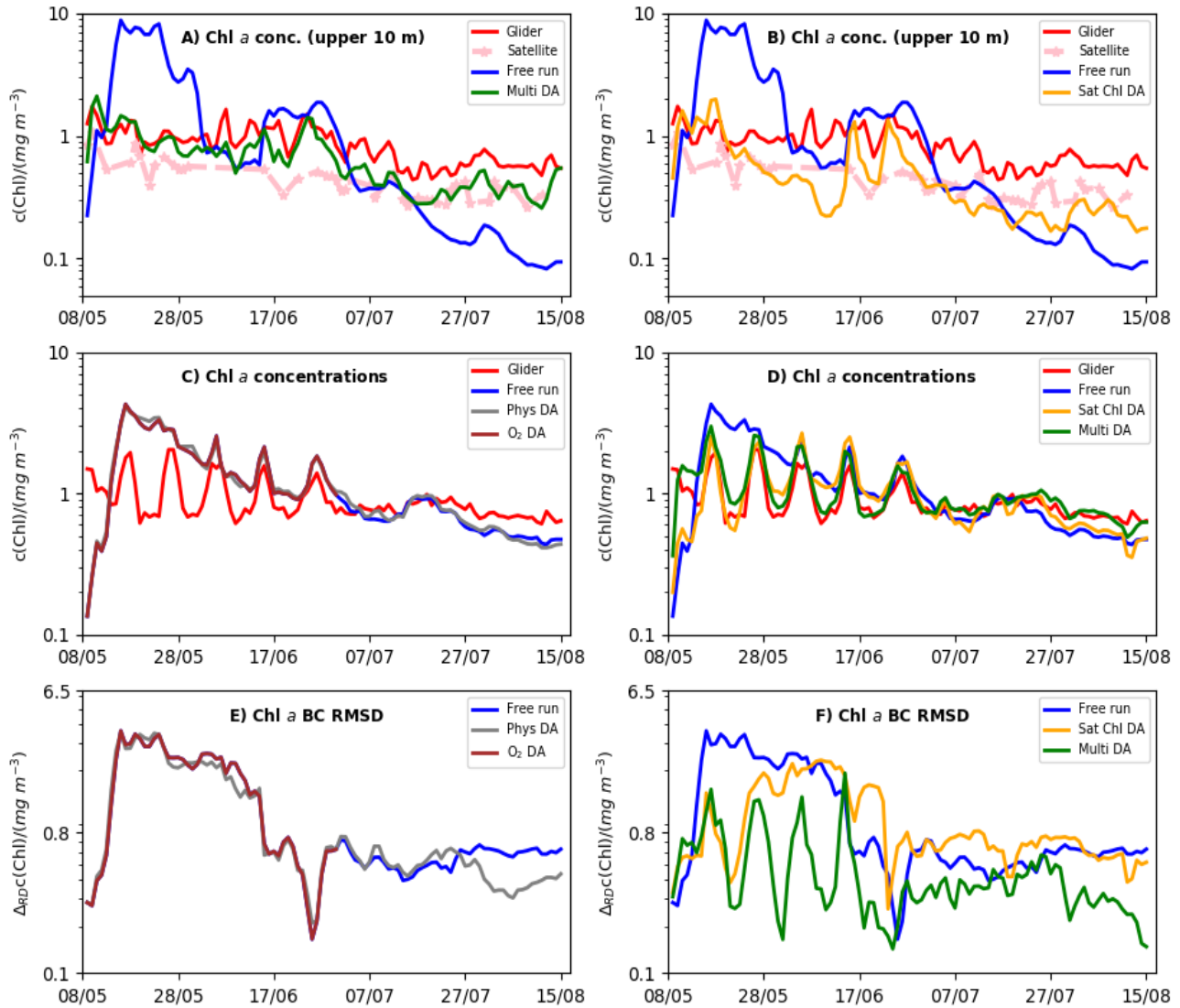
559 Whilst the physical data assimilation improves the model representation of both
 560 temperature and salinity (Figure 6), it is unable to correct the late model spring bloom
 561 (Figure 2) and has a relatively modest impact on chlorophyll concentrations (Figure 3:C,
 562 Figure 5:C,E, Figure 8:E). This can be understood as follows: As the pycnocline is pri-
 563 marily controlled by temperature and salinity, we expect that assimilating the physical
 564 variables may improve vertical gradients in water density and consequently vertical mix-
 565 ing. However, in the well-mixed nutrient-rich waters the onset of the spring bloom de-
 566 pends on the interplay between vertical mixing in the upper oceanic layer and the irra-
 567 diance (e.g. *Huisman et al. (1999)*; *Waniek (2003)*; *Smyth et al. (2014)*). Such interplay
 568 is closely related to the model atmospheric forcing product for the wind stress and the
 569 net incoming short-wave radiation, but an even greater issue is the model response to



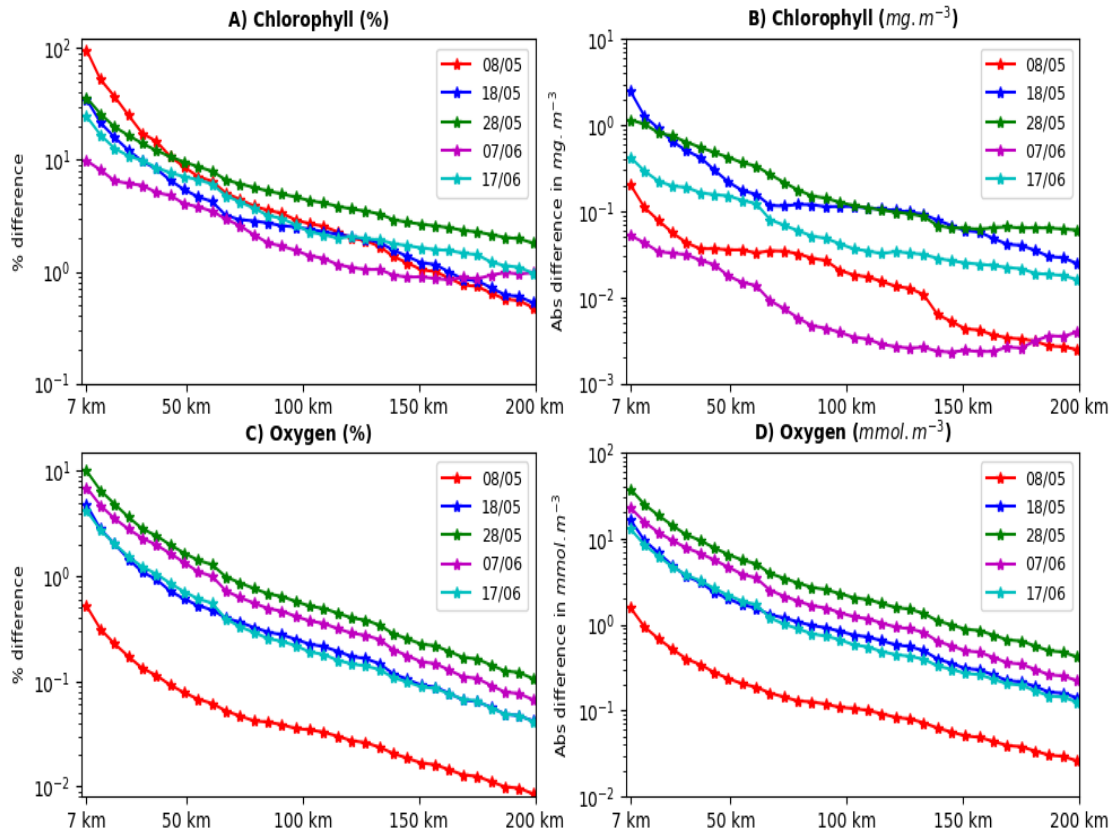
507 **Figure 4.** Comparison of the time median surface chlorophyll *a* distributions (mg m^{-3}) for
 508 the simulation period (08/05 - 15/08, 2018) and the AMM7 domain. The upper two panels show
 509 differences in the mean concentrations between the free run (panel A), the multi-platform re-
 510 analysis (panel B) and the assimilated satellite OC product (the differences are simulated minus
 511 observed chlorophyll). The bottom two panels display the impact of the physical (panel C) and
 512 the glider chlorophyll (panel D) assimilation on the simulated surface chlorophyll *a* concentra-
 513 tions by showing the differences between the two reanalyses and the free run (reanalysis minus
 514 free run). The NWE Shelf-wide impact of the multi-platform assimilation on the surface chloro-
 515 phyll *a* concentrations is dominated by the satellite OC assimilation component (not shown here).
 516 The multi-platform reanalysis (panel B) is therefore almost identical to satellite OC reanalysis.



517 **Figure 5.** The left hand panels (A,C,E,G) demonstrate the spatio-temporal impact of the
 518 multi-platform system components on the simulated chlorophyll *a* concentrations (mg m^{-3}) by
 519 comparing different simulations to the free run. One major advantage of the left-hand side panels
 520 is that they demonstrate how the changes introduced by the assimilation propagate vertically
 521 with the model dynamics, e.g. for the satellite OC assimilation (panel C) that updates the model
 522 only in the mixed layer (the MLD is marked in panels C-D by a yellow line). The right hand
 523 panels (B,D,F,H) show the skill of each component by comparing the simulations to the glider
 524 observations. The first row shows the skill of the free run (panel B) and the required changes to
 525 the free run in order to better match the glider observations (panel A). The rows beneath the
 526 first row compare the chosen reference (free run or glider) with a range of system components:
 527 i) the reanalysis assimilating satellite OC chlorophyll (panels C and D), ii) the reanalysis assimilating
 528 glider chlorophyll (panels E and F) and iii) the multi-platform assimilation (joint physical data,
 529 glider chlorophyll and oxygen, and satellite chlorophyll assimilation, panels G and H).



530 **Figure 6.** The impact of different multi-platform system components on the model chloro-
 531 phyll concentrations. The panels A-B compare the daily chlorophyll values spatially averaged
 532 throughout the upper 10 meters of the water column, within the part of the model domain
 533 visited by the glider. The panels C-D show the daily values spatially averaged throughout the whole
 534 water column, within the part of the model domain visited by the glider (the daily time series
 535 from equation 9), and the remaining panels E-F show the daily BC RMSD (equation 7) for the
 536 same part of the model domain as the panels C-D. The panels display the skill of the following
 537 system components: physical data assimilation (grey color), satellite OC chlorophyll assimilation
 538 (orange) and oxygen assimilation (brown). These components are compared with the multi-
 539 platform assimilative run (joint physical data, glider chlorophyll and oxygen, and satellite OC
 540 chlorophyll assimilation, green color), the free run (blue), the glider observations (red) and the
 541 satellite OC data (pink).



542 **Figure 7.** The horizontal scales for the impact of the glider chlorophyll (panels A-B) and the
 543 glider oxygen (panels C-D) assimilation. The impact of glider assimilation is shown for a range
 544 of days (between 08/05-17/06, 2018). The impact is calculated by comparing the mean absolute
 545 value of the difference in chlorophyll (A-B panels), or oxygen (panels C-D) concentration between
 546 the reanalysis and the model free run. The mean absolute difference is shown relative to the free
 547 run values (in %, panels A,C), or in the absolute values (panels B,D). The absolute difference
 548 was averaged on the circles with 7-200 km radii (the spatial scales shown on the x-axis). The
 549 circles were centered around the glider daily mean location. The mean absolute differences (y-
 550 axis) are shown on a log-scale, a straight-line therefore represents an exponential decrease of the
 551 assimilation impact as a function of spatial scale.

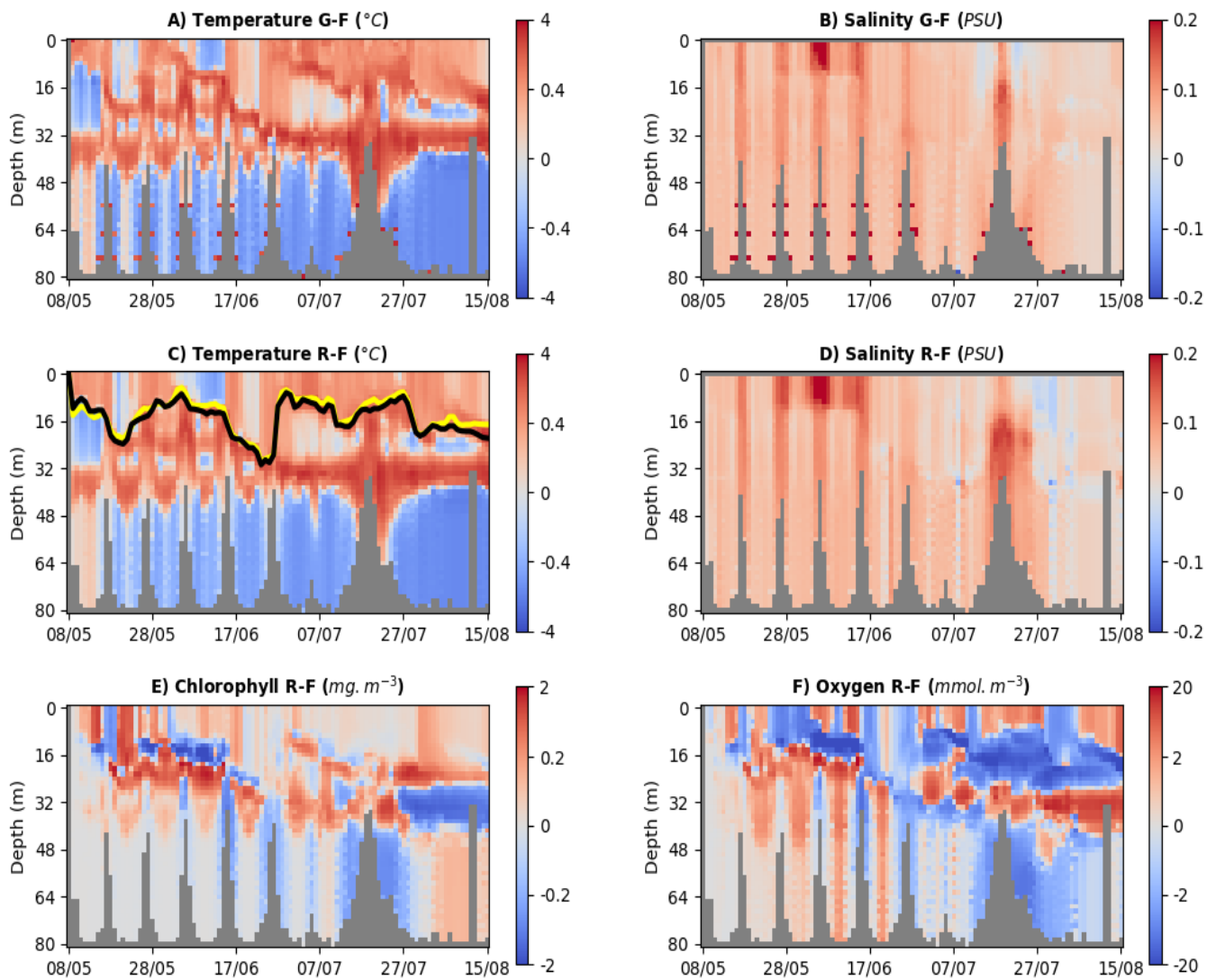
Table 3. The Table demonstrates the skill measured by bias (equation 4), spatial BC RMSD (equation 8) and temporal BC RMSD (equation 10) of the free run and the relative (%) changes to the skill carried by the different assimilative system components. The skill compares the model simulations with the glider data. The percentage changes in the columns for the assimilative runs are calculated relative to the free run skill. The negative percentage means that the bias, or (spatial, temporal) BC RMSD is reduced by the specific system component, whilst the positive percentages mean that bias, or (spatial, temporal) BC RMSD, increases.

variable	free run	phys DA	sat Chl <i>a</i> DA	glid Chl <i>a</i> DA	O ₂ DA	multi DA
Chl <i>a</i> bias	0.31 $mg\ m^{-3}$	+6.8%	-80%	-46.4%	0%	-56.7%
Chl <i>a</i> temporal BC RMSD	0.77 $mg\ m^{-3}$	+5.2%	-54.6%	-70.3%	0%	-65.4%
Chl <i>a</i> spatial BC RMSD	1.14 $mg\ m^{-3}$	-5.5%	-15.3%	-61.9%	0%	-59%
O ₂ bias	25 $mmol\ m^{-3}$	-3.8%	+10.6%	+0.7%	-97%	-98%
O ₂ temporal BC RMSD	13.5 $mmol\ m^{-3}$	-4.3%	+10.8%	-5.4%	-83.8%	-83.7%
O ₂ spatial BC RMSD	29.8 $mmol\ m^{-3}$	-7%	-5.7%	-14.6%	-44.5%	-47.4%

the used atmospheric forcing product, which consists here mostly of the ERSEM underwater light attenuation, the phytoplankton response to specific light conditions and the model vertical mixing scheme. The ERSEM response to the atmospheric forcing is known to be sensitive to the forcing temporal resolution, leading to shifts of up to one week in the timing of the phytoplankton bloom (*Powley et al. (2020)*). Since the assimilation does not alter the atmospheric forcing, the model mixing scheme, or the phytoplankton response to light, assimilating physical data was found to have relatively modest impact on chlorophyll bias, as well as spatial and temporal BC RMSD (between 5-7%, Table 3). However, the impact of physical data assimilation on the simulated phytoplankton could become more substantial within a strongly coupled system (*Goodliff et al. (2019)*). In such system we would mutually update the biogeochemical and the physical increments within a balancing scheme, which could be ideally defined using a two-way coupled physical-biogeochemical model (e.g. *Lengaigne et al. (2007)*). Such development is planned in the foreseeable future.

Finally, we have observed that assimilating glider oxygen into the model has a negligible impact on the simulated chlorophyll concentrations, with a change to the skill metrics of the order $O(10^{-2})$ percent (Table 3, see also Figure 5:C,E). This is expected, as within ERSEM the oxygen variable influences phytoplankton concentrations only indirectly through a complex chain of marine chemical and biological processes (e.g. through influencing remineralization, or nitrification rates, and through the impact of hypoxia on zooplankton).

There is a clear discrepancy between the oxygen time series of the glider and the model free run (Figure 9, Figure 10:A-B), with glider oxygen concentrations steadily decreasing, while the simulated oxygen peaks in late May (Figure 10:A-B). Furthermore, simulated oxygen concentrations have a substantial positive bias (25 $mmol\ m^{-3}$, Table 3, Figure 10:A-B) relative to the glider observations. Figure 9:A clearly shows that photosynthesis is an important driver of the simulated oxygen, producing a large oxygen surge in the mixed layer during the simulated late spring bloom. Some connection between oxygen and chlorophyll concentrations (a proxy for primary productivity) appears also in the glider observations (Figure 9:B), with the peak in oxygen concentrations located in



584 **Figure 8.** Hovmöller diagrams to demonstrate the impact of physical (SST, in situ temper-
 585 ature and salinity, including Cabot glider data) assimilation on the model variables. The upper
 586 row (A and B) shows the difference between glider ("G" in the title) and free run ("F") outputs
 587 for temperature (A) and salinity (B). The middle row (C and D) shows differences for the same
 588 variables between physical reanalysis ("R") and the free run. The bottom row (E and F) shows
 589 the same differences between physical reanalysis and the free run, but for the two biogeochemical
 590 variables addressed by this study: total chlorophyll and oxygen. The two lines in the panel C
 591 compare the mixed layer depth of the free run (yellow) and of the physical reanalysis (black).
 592 The mixed layer depth has been obtained in both cases from the model outputs.

609 the neighborhood of the glider deep chlorophyll maxima (Figure 3:B). As for chlorophyll,
610 a simple way to improve simulated oxygen is to assimilate the glider oxygen data into
611 the model (Figure 10:D, Figure 11:H). Assimilating glider oxygen into the model reduces
612 the oxygen bias by 97%, temporal BC RMSD by 84% and spatial BC RMSD by 45% (Ta-
613 ble 3). However, as in the case of chlorophyll, such assimilation has a limited spatial im-
614 pact on the NWE Shelf (Figure 7:C-D and Figure 12:C). Unlike chlorophyll, the glider
615 oxygen assimilation horizontal impact reduces with spatial scale at a rate largely inde-
616 pendent of time (Figure 7:C-D). Beyond the 50 km scale the assimilation horizontal im-
617 pact decays approximately exponentially (a straight line in Figure 7:C-D), with a halv-
618 ing scale of approximately 40 km, which means the impact is reduced by an order of mag-
619 nitude at a 130 km scale.

620 Since the modeled oxygen concentrations are largely driven by the phytoplankton
621 seasonal cycle, it is not surprising that assimilation of either satellite OC, or glider chloro-
622 phyll, has a major influence on the simulated oxygen (Figure 11:C,E, Figure 12:B). The
623 assimilated chlorophyll modifies the simulated oxygen after a necessary time-lag, remov-
624 ing the excess oxygen from the model spring bloom and generating some deep oxygen
625 maxima in early-to-mid June (Figure 11:C-F). The chlorophyll assimilation consistently
626 improves oxygen in the period up to the start of June, but typically degrades oxygen in
627 early-to-mid June (Figure 10:B,D,F), mostly due to the surge in oxygen concentrations
628 around the deep oxygen maxima (Figure 11:C,E). The oxygen surge is likely to be partly
629 driven by the deep chlorophyll maxima, e.g. by the overestimated chlorophyll concen-
630 trations around the deep maxima in the satellite OC assimilation (Figure 5:D). However,
631 other drivers such as zooplankton and bacteria respiration are likely to contribute to the
632 deep oxygen maxima. The mechanism for this is suggested by Figure 13:C-F: the chloro-
633 phyll assimilation removes phytoplankton biomass from the mixed layer, limiting the re-
634 sources for the simulated zooplankton and bacteria, and reducing their concentrations.
635 The reduced phytoplankton concentrations seem to have much larger and more consis-
636 tent impact on the zooplankton concentrations than on bacteria (Figure 13:C-F) and the
637 reduced zooplankton concentration means less oxygen is removed through respiration,
638 which likely produces excess oxygen concentrations.

639 Compared to chlorophyll assimilation, the physical data assimilation has a relatively
640 modest impact on the simulated oxygen (Figure 8:F, Figure 12:A-B), but it tends to con-
641 sistent improve both the oxygen bias, and the spatial and temporal BC RMSD (by 3–
642 7%, Table 3). The impact of physical data assimilation on the oxygen concentrations can
643 be explained by the lowered oxygen saturation concentrations under the increase in tem-
644 perature within the reanalysis (Figure 8:C).

645 Finally, we have combined all the assimilative system components (physical data
646 assimilation, satellite OC, glider chlorophyll and oxygen) into a multi-platform assimi-
647 lative run and we have shown that multi-platform assimilation has the capability to op-
648 timally combine the skill of all its components (Figure 4:B, Figure 6:D,F, Figure 9:D-
649 E, Table 3). The multi-platform chlorophyll re-analysis is dominated in the vicinity of
650 the glider by the glider chlorophyll assimilative component (Figure 5:E,G), whilst fur-
651 ther away from the glider it is dominated by the satellite OC assimilation (Figure 4:D).
652 The multi-platform oxygen re-analysis is dominated near the glider locations by the glider
653 oxygen assimilation (Figure 10:D), whilst further away from the glider locations it is do-
654 minantly shaped by the satellite OC assimilation (Figure 12:B,D).

652 4 Summary

653 Present and future glider missions on the NWE Shelf will provide us with three-
654 dimensional (3D) data on some specific biogeochemical variables (presently mostly for
655 chlorophyll and oxygen) combined with physical measurements (e.g. temperature and
656 salinity). These data will be, together with satellite missions, integrated into our ecosys-

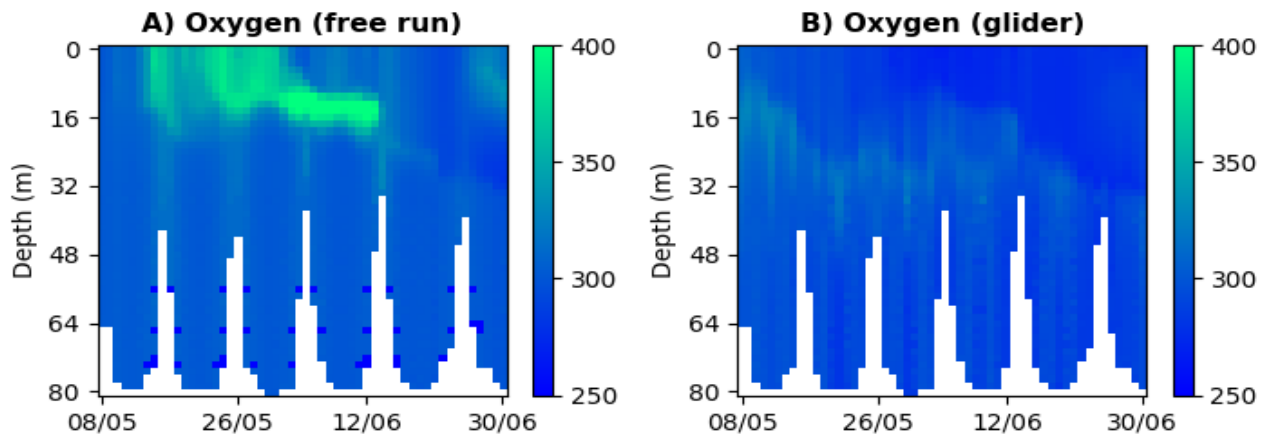
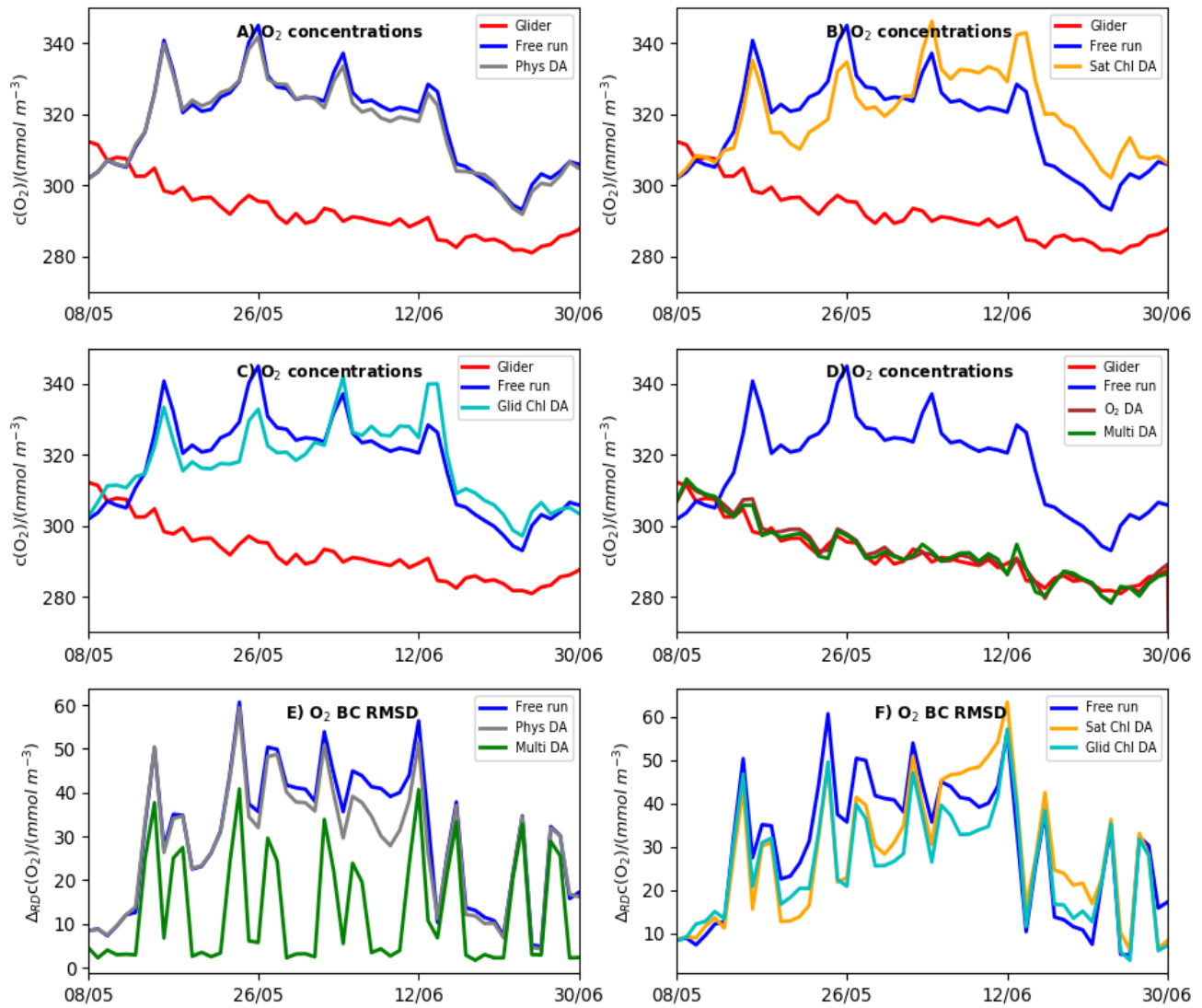


Figure 9. Hovmöller diagrams for the model free run and the glider observations. The left-hand panel (A) shows the model free run outputs for oxygen (mmol m^{-3}) horizontally averaged through the area covered by the glider during each day (the plot is depth vs time). The right-hand panel (B) shows the same for the glider-observed oxygen.

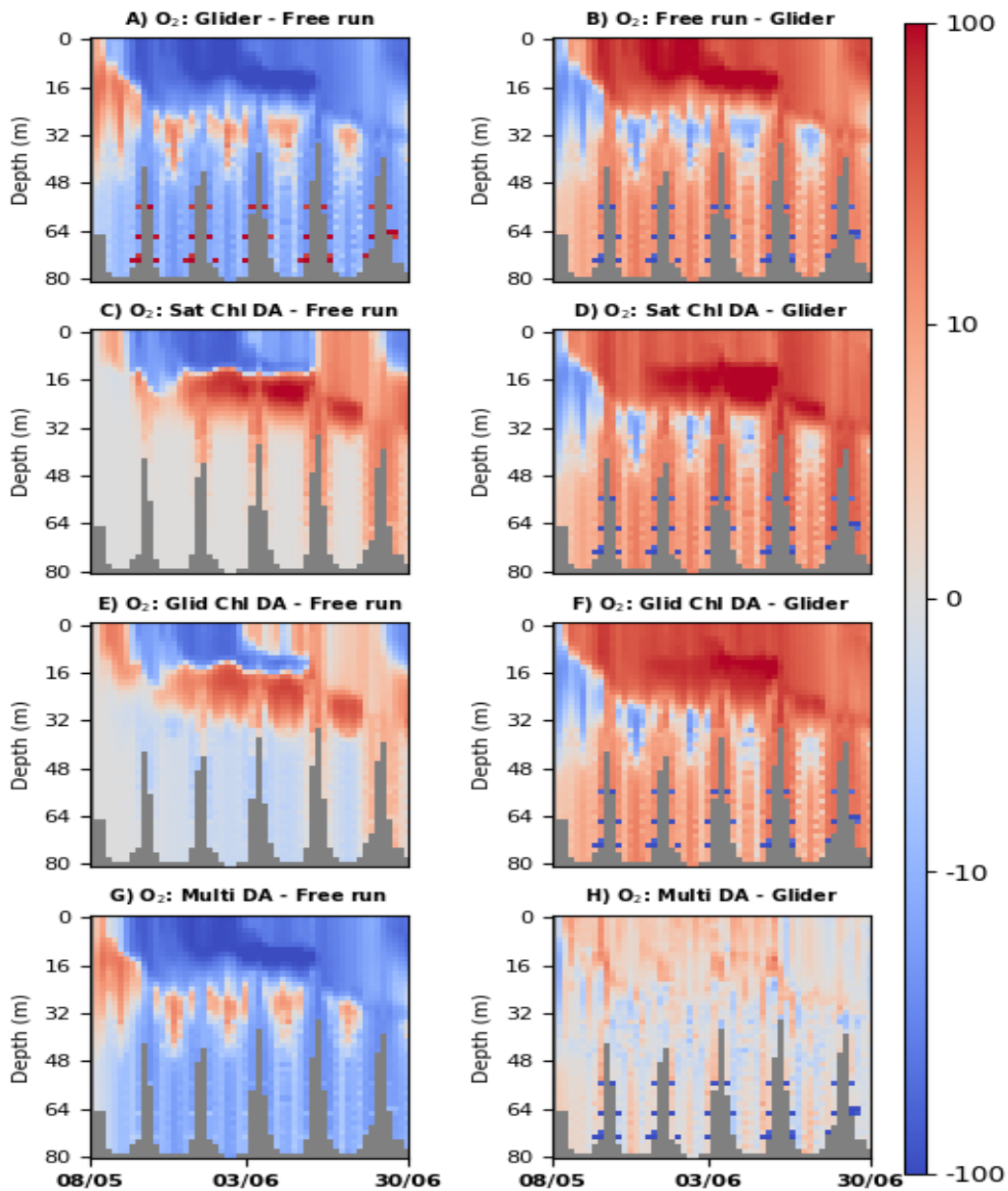
tem models by means of a multi-platform assimilative system. It is of crucial importance to understand what observed variables need to be assimilated in order to represent well a target ecosystem indicator, and what assimilation may need to be avoided because it can paradoxically degrade the model skill for the target indicator. Furthermore, different data will be available for different spatial and temporal regions on the NWE Shelf and it is essential to understand how the limitations imposed by the availability of the observational data impact on the quality of the multi-platform reanalyses. To address these questions we explored the impact of different system components (physical data, satellite OC chlorophyll, glider chlorophyll and oxygen assimilation) on the simulated ecosystem state, using the operational set-up currently assimilating physical variables and satellite OC chlorophyll. This study has taught us several important lessons:

a) Assimilating physical data (SST, in situ temperature and salinity) has a negligible impact on the simulated phytoplankton bloom. This is because the modeled phytoplankton bloom depends in the North Sea mostly on the model response to the atmospheric forcing (wind stress and solar radiance), which remains unchanged by the temperature and salinity assimilation. Since the phytoplankton bloom is an essential driver of the ecosystem dynamics on the NWE Shelf (*Henson et al. (2009)*), it is quite likely that physical glider data assimilation has a relatively minor importance for the simulated ecosystem dynamics on the NWE Shelf. This is quite different from some other global regions where physical assimilation is either desirable (*Anderson et al. (2000)*; *Yu et al. (2018)*), or can degrade the biogeochemical model skill (*Berline et al. (2007)*; *Holt et al. (2014)*; *Raghukumar et al. (2015)*; *Park et al. (2018)*). Based on this study we would suggest that, at least around the spring bloom in the North Sea, physical assimilation can be used to improve the physical model skill, whilst its impact on the coupled biogeochemical model can be relatively ignored.

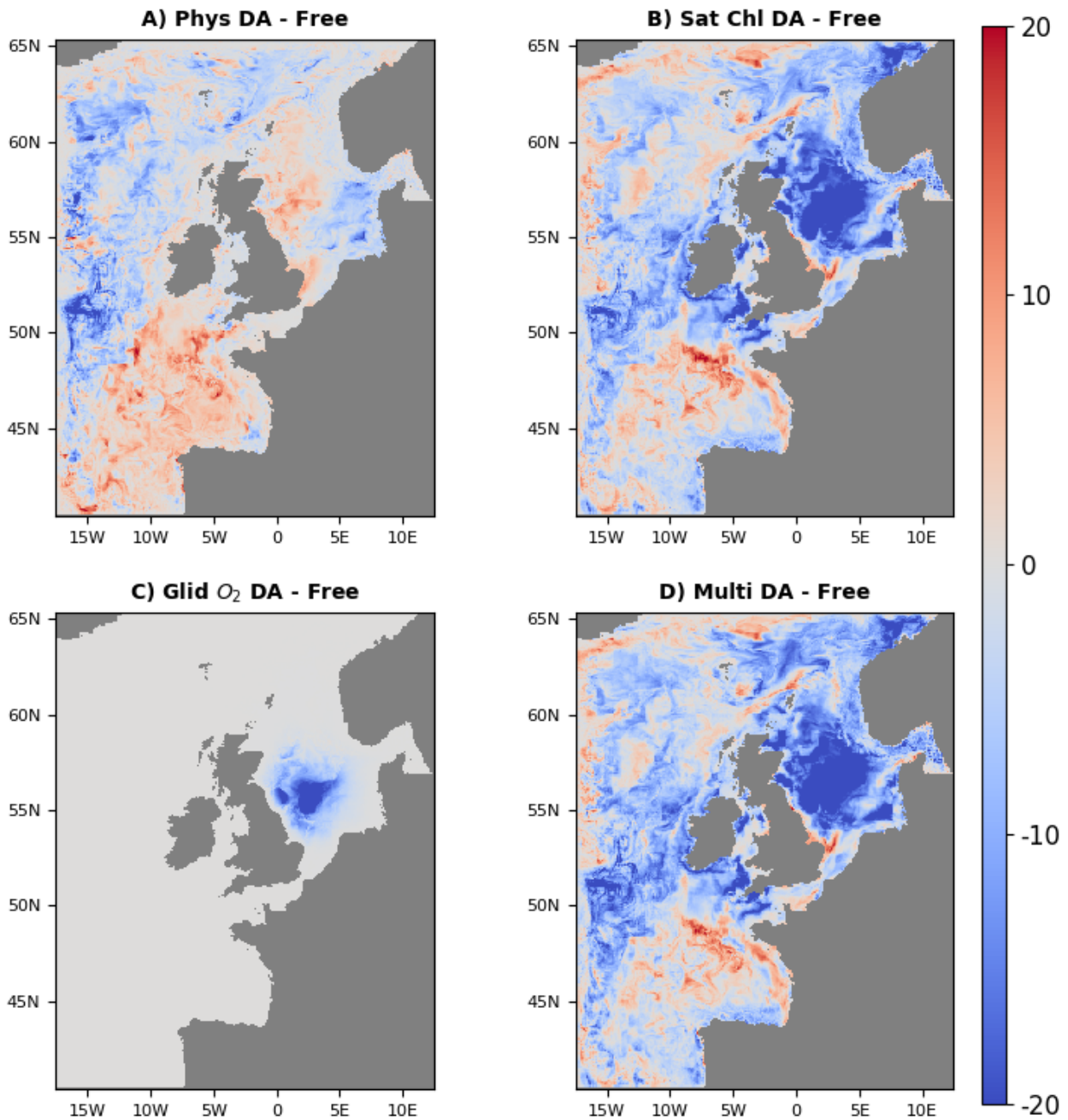
b) In terms of chlorophyll, the glider chlorophyll assimilation is the dominant and best performing component of the multi-platform assimilative system within the 50 km horizontal proximity of the glider. Further away from the glider locations, assimilating satellite OC data substantially improves the surface chlorophyll concentrations, but it can also produce realistic updates to the sub-surface chlorophyll. Since satellite OC assimilation updates chlorophyll only within the mixed layer, the updates to the sub-surface



659 **Figure 10.** The impact of different multi-platform system components on the model oxygen.
 660 The panels A-D compare the daily oxygen values spatially averaged throughout the whole water
 661 column, within the part of the model domain visited by the glider (the daily time series from
 662 equation 9), and the panels E-F show the daily BC RMSD (equation 7). The panels display the
 663 skill of the following system components: physical data assimilation (grey color), satellite OC
 664 chlorophyll assimilation (orange), glider chlorophyll assimilation (light blue) and oxygen assi-
 665 milation (brown). These components are compared with the multi-platform assimilative run (joint
 666 physical data, glider chlorophyll and oxygen, and satellite chlorophyll assimilation, green color),
 667 the free run (blue) and the glider observations (red).

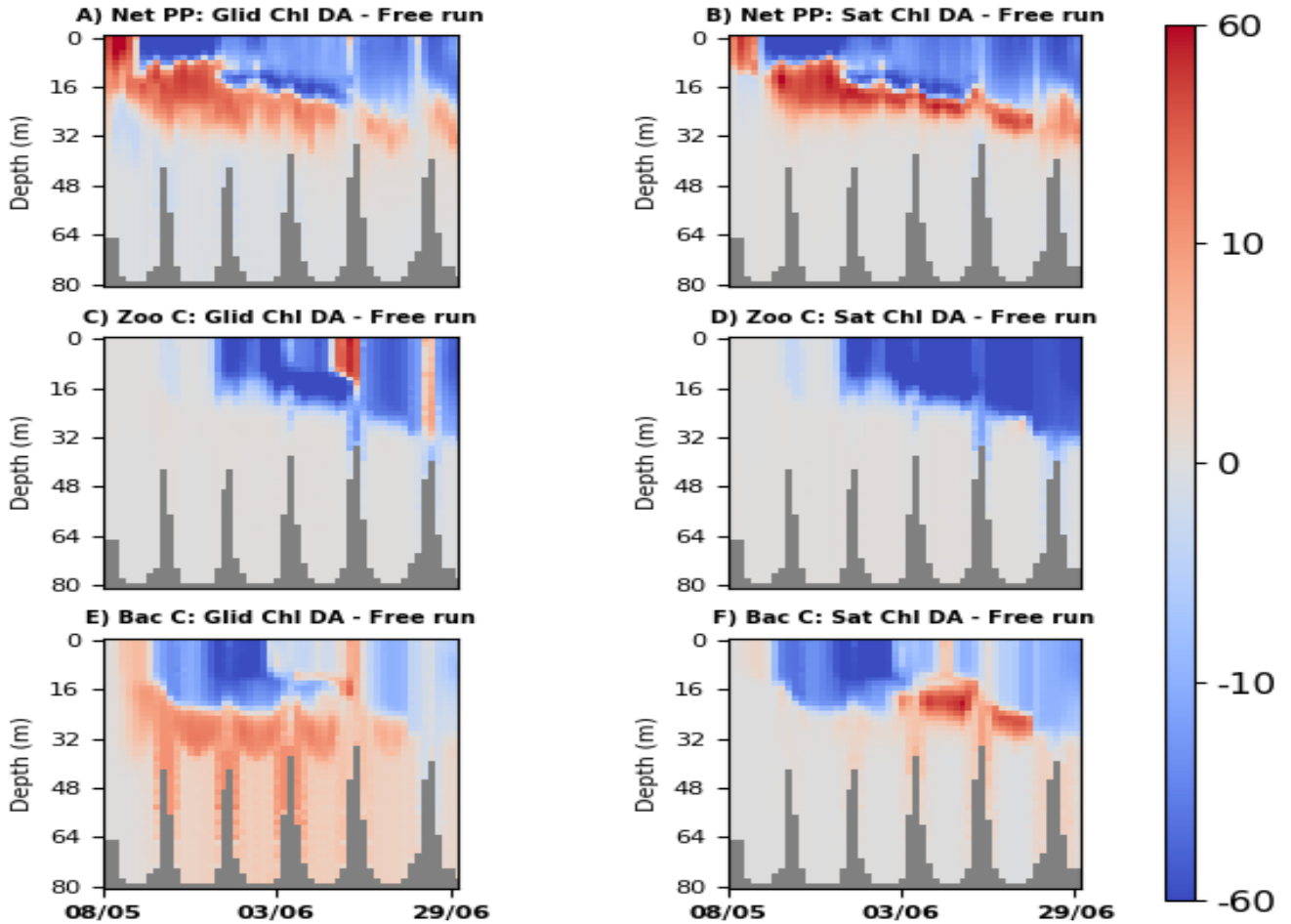


668 **Figure 11.** The left hand panels (A,C,E,G) demonstrate the impact of the multi-platform
 669 system components on the simulated oxygen concentrations (mmol m^{-3}) by comparing different
 670 simulations to the free run. These panels are particularly well suited to see how chlorophyll as-
 671 similation dynamically influences the simulated oxygen. The right hand panels (B,D,F,H) show
 672 the skill of each component by comparing the simulations to the glider observations. The first
 673 row shows the skill of the free run (panel B) and the required changes to the free run in order
 674 to better match the glider observations (panel A). The rows beneath the first row compare the
 675 chosen reference (free run or glider) with a range of system components: i) the reanalysis assi-
 676 milating satellite OC chlorophyll (panels C and D), ii) the reanalysis assimilating glider chlorophyll
 677 (panels E and F) and iii) the multi-platform assimilation (joint physical data, glider chlorophyll
 678 and oxygen, and satellite chlorophyll assimilation) (panels G and H).



679 **Figure 12.** Comparison of the time median surface oxygen distributions (mmol m^{-3}) for the
 680 oxygen glider data period (08/05/2018 - 29/06, 2018). The panels show the impact of the dif-
 681 ferent multi-platform system components on the modelled oxygen by comparing the differences
 682 between four reanalyses and the free run. The reanalyses presented in the panels are the physical
 683 data assimilation (panel A), the OC satellite chlorophyll assimilation (panel B), the glider oxygen
 684 assimilation (panel C) and the multi-platform assimilation (panel D).

-24-



685 **Figure 13.** The different panels help to interpret the impact of the simulated primary pro-
 686 duction and respiration on the modeled oxygen concentrations. We show the difference between
 687 the glider chlorophyll assimilation (left-hand side panels, A,C,E), or OC chlorophyll assimilation
 688 (right-hand side panels, B,D,F) and the model free run (always assimilative run minus free run).
 689 The difference is shown for (i) the total net primary production ($\text{mg C m}^{-3}\text{day}^{-1}$, panels A-B),
 690 (ii) total zooplankton carbon concentrations (mg C m^{-3} , panels C-D) and (iii) heterotrophic
 691 bacteria carbon concentrations (mg C m^{-3} , panels E-F).

728 chlorophyll are explained by the model dynamical response to the assimilation. The skill
 729 of satellite OC assimilation in sub-surface chlorophyll is important, as glider technology
 730 will be able to cover only limited parts of the NWE Shelf and future multi-platform as-
 731 similative system will have to rely heavily on satellite data.

732 c) The modelled phytoplankton dynamics is impacted by the oxygen concentrations
 733 only indirectly, e.g. through remineralization, or nitrification rates and the impact of hy-
 734 poxia on zooplankton (*Butenschön et al. (2016)*). It is therefore hardly surprising that
 735 univariate assimilation of oxygen has a negligible impact on the simulated phytoplank-
 736 ton chlorophyll concentrations. This also means that one can assimilate oxygen into ERSEM
 737 without worrying about its consequences for the modelled phytoplankton. Such an oxy-
 738 gen assimilation has an obvious advantage in that it outperforms any other run in the
 739 model simulation of oxygen.

740 d) Two important drivers of the simulated oxygen concentrations are the primary
 741 production and respiration. Consequently, assimilating (satellite OC, or glider) chloro-
 742 phyll was found to have a major impact on the modeled oxygen. The removal of the late
 743 model bloom in the reanalysis improves the modeled oxygen, however it produces spu-
 744 rious deep oxygen maxima, partly due to the productivity at the deep chlorophyll max-
 745 ima and partly due to the reduced respiration by the ERSEM zooplankton. Physical data
 746 assimilation has a stronger impact on the oxygen than on chlorophyll (oxygen satura-
 747 tion levels depend substantially on temperature), but it had substantially less impact
 748 on the simulated oxygen than the chlorophyll assimilation.

749 e) The multi-platform assimilation (joint physical data, glider chlorophyll and oxy-
 750 gen, satellite OC chlorophyll assimilation) combines optimally the skill of its components
 751 and always performs comparably to, or better than its best performing component.

752 f) Based on the results of this study we expect that the multi-platform system will
 753 provide us with improved-quality operational products on the NWE Shelf.

754 Acknowledgments

755 This work was supported by a joint effort of Natural Environment Research Coun-
 756 cil (NERC) funded projects of the Marine Integrated Autonomous Observing Systems
 757 (MIAOS) programme: Combining Autonomous observations and Models for Predicting
 758 and Understanding Shelf seas (CAMPUS) and Alternative Framework to Assess Marine
 759 Ecosystem Functioning in Shelf Seas (AlterECO, <http://projects.noc.ac.uk/altereco/>),
 760 grant no. NE/P013899/1. The work also benefited from the Copernicus Marine Envi-
 761 ronment Monitoring Service (CMEMS) funded projects OPTical data Modelling and As-
 762 similation (OPTIMA) and NOWMAPS. The work contributes to the SEAMLESS project,
 763 which received funding from the European Union’s Horizon 2020 research and innova-
 764 tion programme under grant agreement no. 101004032. This work was also supported
 765 by the UK National Centre for Earth Observation (NCEO). The European Regional Seas
 766 Ecosystem Model (ERSEM) code v20.10 can be publicly traced on <https://doi.org/10.5281/zenodo.4075315>
 767 and the Framework for Aquatic Biogeochemical Models (FABM) v1.0 on [https://doi.org/10.5281/-](https://doi.org/10.5281/zenodo.4075315)
 768 [zenodo.4075315](https://doi.org/10.5281/zenodo.4075315). We thank the European Space Agency Climate Initiative “Ocean Color”
 769 (<https://esa-oceancolour-cci.org/>) for providing the ocean color data. The glider data
 770 used in the study (doi:10.5285/b57d215e-065f-7f81-e053-6c86abc01a82) are publicly avail-
 771 able on https://www.bodc.ac.uk/data/published_data_library/catalogue/. The model was
 772 forced by atmospheric ERA5 product of The European Centre for Medium-Range Weather
 773 Forecasts (ECMWF, <https://www.ecmwf.int/>). The river forcing data used by the model
 774 were prepared by Sonja van Leeuwen and Helen Powley as part of UK Shelf Seas Bio-
 775 geochemistry programme (contract no. NE/K001876/1) of the NERC and the Depart-
 776 ment for Environment Food and Rural Affairs (DEFRA). We acknowledge use of the MON-
 777 Soon system, a collaborative facility supplied under the Joint Weather and Climate Re-

778 search Programme, a strategic partnership between the Met Office and the NERC. The
 779 different outputs for the free run simulations and reanalyses are stored on the MONSooN
 780 storage facility MASS and can be obtained upon request.

781 References

- 782 Allen, J., M. Eknes, and G. Evensen (2003), An ensemble kalman filter with a com-
 783 plex marine ecosystem model: hindcasting phytoplankton in the cretan sea, in
 784 *Annales Geophysicae*, vol. 21, pp. 399–411.
- 785 Anderson, L. A., A. R. Robinson, and C. J. Lozano (2000), Physical and biological
 786 modeling in the gulf stream region:: I. data assimilation methodology, *Deep Sea*
 787 *Research Part I: Oceanographic Research Papers*, 47(10), 1787–1827.
- 788 Andersson, E. (2003), Modelling the temporal evolution of innovation statistics, *This*
 789 *volume*, pp. 153–164.
- 790 Artioli, Y., J. C. Blackford, M. Butenschön, J. T. Holt, S. L. Wakelin, H. Thomas,
 791 A. V. Borges, and J. I. Allen (2012), The carbonate system in the north sea: Sen-
 792 sitivity and model validation, *Journal of Marine Systems*, 102, 1–13.
- 793 Baretta, J., W. Ebenhöh, and P. Ruardij (1995), The european regional seas ecosys-
 794 tem model, a complex marine ecosystem model, *Netherlands Journal of Sea Re-*
 795 *search*, 33(3-4), 233–246.
- 796 Baretta-Bekker, J., J. Baretta, and W. Ebenhöh (1997), Microbial dynamics in the
 797 marine ecosystem model ersem ii with decoupled carbon assimilation and nutrient
 798 uptake, *Journal of Sea Research*, 38(3-4), 195–211.
- 799 Bell, M. J., A. Schiller, P.-Y. Le Traon, N. Smith, E. Dombrowsky, and K. Wilmer-
 800 Becker (2015), An introduction to godae oceanview.
- 801 Berline, L., J.-M. Brankart, P. Brasseur, Y. Ourmières, and J. Verron (2007), Im-
 802 proving the physics of a coupled physical–biogeochemical model of the north
 803 atlantic through data assimilation: Impact on the ecosystem, *Journal of Marine*
 804 *Systems*, 64(1-4), 153–172.
- 805 Biermann, L., C. Guinet, M. N. Bester, A. Brierley, and L. Boehme (2015), An
 806 alternative method for correcting fluorescence quenching.
- 807 Bittig, H. C., B. Fiedler, R. Scholz, G. Krahnmann, and A. Körtzinger (2014), Time
 808 response of oxygen optodes on profiling platforms and its dependence on flow
 809 speed and temperature, *Limnology and Oceanography: Methods*, 12(8), 617–636.
- 810 Blackford, J. (1997), An analysis of benthic biological dynamics in a north sea
 811 ecosystem model, *Journal of Sea Research*, 38(3-4), 213–230.
- 812 Bloom, S., L. Takacs, A. Da Silva, and D. Ledvina (1996), Data assimilation using
 813 incremental analysis updates, *Monthly Weather Review*, 124(6), 1256–1271.
- 814 Borges, A., L.-S. Schiettecatte, G. Abril, B. Delille, and F. Gazeau (2006), Carbon
 815 dioxide in european coastal waters, *Estuarine, Coastal and Shelf Science*, 70(3),
 816 375–387.
- 817 Bruggeman, J., and K. Bolding (2014), A general framework for aquatic biogeochem-
 818 ical models, *Environmental modelling & software*, 61, 249–265.
- 819 Butenschön, M., J. Clark, J. N. Aldridge, J. I. Allen, Y. Artioli, J. Blackford,
 820 J. Bruggeman, P. Cazenave, S. Ciavatta, S. Kay, et al. (2016), Ersem 15.06: a
 821 generic model for marine biogeochemistry and the ecosystem dynamics of the
 822 lower trophic levels, *Geoscientific Model Development*, 9(4), 1293–1339.
- 823 Campbell, J. W. (1995), The lognormal distribution as a model for bio-optical vari-
 824 ability in the sea, *Journal of Geophysical Research: Oceans*, 100(C7), 13,237–
 825 13,254.
- 826 Carmillet, V., J.-M. Brankart, P. Brasseur, H. Drange, G. Evensen, and J. Verron
 827 (2001), A singular evolutive extended kalman filter to assimilate ocean color data
 828 in a coupled physical–biochemical model of the north atlantic ocean, *Ocean Mod-*
 829 *elling*, 3(3-4), 167–192.

- 830 Ciavatta, S., R. Torres, S. Saux-Picart, and J. I. Allen (2011), Can ocean color as-
831 simulation improve biogeochemical hindcasts in shelf seas?, *Journal of Geophysical*
832 *Research: Oceans*, 116(C12).
- 833 Ciavatta, S., R. Torres, V. Martinez-Vicente, T. Smyth, G. Dall'Olmo, L. Polimene,
834 and J. I. Allen (2014), Assimilation of remotely-sensed optical properties to im-
835 prove marine biogeochemistry modelling, *Progress in oceanography*, 127, 74–95.
- 836 Ciavatta, S., S. Kay, S. Saux-Picart, M. Butenschön, and J. Allen (2016), Decadal
837 reanalysis of biogeochemical indicators and fluxes in the north west european
838 shelf-sea ecosystem, *Journal of Geophysical Research: Oceans*, 121(3), 1824–1845.
- 839 Ciavatta, S., R. Brewin, J. Skakala, L. Polimene, L. de Mora, Y. Artioli, and J. I.
840 Allen (2018), Assimilation of ocean-color plankton functional types to improve
841 marine ecosystem simulations, *Journal of Geophysical Research: Oceans*, 123(2),
842 834–854.
- 843 Ciavatta, S., S. Kay, R. Brewin, R. Cox, A. Di Cicco, F. Nencioli, L. Polimene,
844 M. Sammartino, R. Santoleri, J. Skákala, et al. (2019), Ecoregions in the mediter-
845 ranean sea through the reanalysis of phytoplankton functional types and carbon
846 fluxes, *Journal of Geophysical Research: Oceans*.
- 847 Cossarini, G., P. Lermusiaux, and C. Solidoro (2009), Lagoon of venice ecosys-
848 tem: Seasonal dynamics and environmental guidance with uncertainty analyses
849 and error subspace data assimilation, *Journal of Geophysical Research: Oceans*,
850 114(C6).
- 851 Cossarini, G., L. Mariotti, L. Feudale, A. Mignot, S. Salon, V. Taillandier,
852 A. Teruzzi, and F. D'Ortenzio (2019), Towards operational 3d-var assimilation
853 of chlorophyll biogeochemical-argo float data into a biogeochemical model of the
854 mediterranean sea, *Ocean Modelling*, 133, 112–128.
- 855 Desroziers, G., L. Berre, B. Chapnik, and P. Poli (2005), Diagnosis of observation,
856 background and analysis-error statistics in observation space, *Quarterly Journal*
857 *of the Royal Meteorological Society: A journal of the atmospheric sciences, applied*
858 *meteorology and physical oceanography*, 131(613), 3385–3396.
- 859 Doney, S. C. (1999), Major challenges confronting marine biogeochemical modeling,
860 *Global Biogeochemical Cycles*, 13(3), 705–714.
- 861 Doney, S. C., K. Lindsay, K. Caldeira, J.-M. Campin, H. Drange, J.-C. Dutay,
862 M. Follows, Y. Gao, A. Gnanadesikan, N. Gruber, et al. (2004), Evaluating global
863 ocean carbon models: The importance of realistic physics, *Global Biogeochemical*
864 *Cycles*, 18(3).
- 865 El Moussaoui, A., C. Perruche, E. Greiner, C. Ethé, and M. Gehlen (2011), Integra-
866 tion of biogeochemistry into mercator ocean systems, *Mercator Océan Newsletter*,
867 40, 3–14.
- 868 Fontana, C., C. Grenz, and C. Pinazo (2010), Sequential assimilation of a year-long
869 time-series of seawifs chlorophyll data into a 3d biogeochemical model on the
870 french mediterranean coast, *Continental Shelf Research*, 30(16), 1761–1771.
- 871 Ford, D. (2020), Assimilating synthetic biogeochemical-argo and ocean colour ob-
872 servations into a global ocean model to inform observing system design, *submitted*
873 *to Biogeosciences*, freely available at [https://www.biogeosciences-discuss.net/bg-](https://www.biogeosciences-discuss.net/bg-2020-152/bg-2020-152/bg-2020-152.pdf)
874 [2020-152/bg-2020-152.pdf](https://www.biogeosciences-discuss.net/bg-2020-152/bg-2020-152.pdf).
- 875 Ford, D., and R. Barciela (2017), Global marine biogeochemical reanalyses assim-
876 ilating two different sets of merged ocean colour products, *Remote Sensing of*
877 *Environment*, 203, 40–54.
- 878 Ford, D., K. Edwards, D. Lea, R. Barciela, M. Martin, and J. Demaria (2012),
879 Assimilating globcolour ocean colour data into a pre-operational physical-
880 biogeochemical model, *Ocean Science*, 8(5), 751–771.
- 881 Ford, D. A., J. van der Molen, K. Hyder, J. Bacon, R. Barciela, V. Creach, R. McE-
882 wan, P. Ruardij, and R. Forster (2017), Observing and modelling phytoplankton
883 community structure in the north sea, *Biogeosciences*, 14(6), 1419–1444.

- 884 Friedlingstein, P., P. Cox, R. Betts, L. Bopp, W. von Bloh, V. Brovkin, P. Cadule,
885 S. Doney, M. Eby, I. Fung, et al. (2006), Climate–carbon cycle feedback analy-
886 sis: results from the c4mip model intercomparison, *Journal of climate*, *19*(14),
887 3337–3353.
- 888 Garcia, H. E., R. A. Locarnini, T. P. Boyer, J. I. Antonov, O. K. Baranova, M. M.
889 Zweng, J. R. Reagan, D. R. Johnson, A. V. Mishonov, and S. Levitus (2013),
890 World ocean atlas 2013. volume 4, dissolved inorganic nutrients (phosphate, ni-
891 trate, silicate).
- 892 Geider, R., H. MacIntyre, and T. Kana (1997), Dynamic model of phytoplankton
893 growth and acclimation: responses of the balanced growth rate and the chloro-
894 phyll a: carbon ratio to light, nutrient-limitation and temperature, *Marine Ecol-
895 ogy Progress Series*, *148*, 187–200.
- 896 Germaineaud, C., J.-M. Brankart, and P. Brasseur (2019), An ensemble-based prob-
897 abilistic score approach to compare observation scenarios: an application to
898 biogeochemical-argo deployments, *Journal of Atmospheric and Oceanic Tech-
899 nology*, (2019).
- 900 Good, S. A., M. J. Martin, and N. A. Rayner (2013), En4: Quality controlled ocean
901 temperature and salinity profiles and monthly objective analyses with uncertainty
902 estimates, *Journal of Geophysical Research: Oceans*, *118*(12), 6704–6716.
- 903 Goodliff, M., T. Bruening, F. Schwichtenberg, X. Li, A. Lindenthal, I. Lorkowski,
904 and L. Nerger (2019), Temperature assimilation into a coastal ocean-
905 biogeochemical model: assessment of weakly and strongly coupled data assimi-
906 lation, *Ocean Dynamics*, *69*(10), 1217–1237.
- 907 Gregg, W. W. (2008), Assimilation of seawifs ocean chlorophyll data into a three-
908 dimensional global ocean model, *Journal of Marine Systems*, *69*(3-4), 205–225.
- 909 Gregg, W. W., and C. S. Rousseaux (2017), Simulating pace global ocean radiances,
910 *Frontiers in Marine Science*, *4*, 60.
- 911 Hemsley, V. S., T. J. Smyth, A. P. Martin, E. Frajka-Williams, A. F. Thompson,
912 G. Damerell, and S. C. Painter (2015), Estimating oceanic primary production
913 using vertical irradiance and chlorophyll profiles from ocean gliders in the north
914 atlantic, *Environmental science & technology*, *49*(19), 11,612–11,621.
- 915 Henson, S. A., J. P. Dunne, and J. L. Sarmiento (2009), Decadal variability in
916 north atlantic phytoplankton blooms, *Journal of Geophysical Research: Oceans*,
917 *114*(C4).
- 918 Hinrichs, I., V. Gouretski, J. Pätch, K. Emeis, and D. Stammer (2017), North sea
919 biogeochemical climatology.
- 920 Hollingsworth, A., and P. Lönnberg (1986), The statistical structure of short-range
921 forecast errors as determined from radiosonde data. part i: The wind field, *Tellus*
922 *A*, *38*(2), 111–136.
- 923 Holt, J., J. I. Allen, T. R. Anderson, R. Brewin, M. Butenschön, J. Harle, G. Huse,
924 P. Lehodey, C. Lindemann, L. Memery, et al. (2014), Challenges in integrative
925 approaches to modelling the marine ecosystems of the north atlantic: Physics to
926 fish and coasts to ocean, *Progress in Oceanography*, *129*, 285–313.
- 927 Holte, J., and L. Talley (2009), A new algorithm for finding mixed layer depths
928 with applications to argo data and subantarctic mode water formation, *Journal of*
929 *Atmospheric and Oceanic Technology*, *26*(9), 1920–1939.
- 930 Hoteit, I., G. Triantafyllou, G. Petihakis, and J. Allen (2003), A singular evolutive
931 extended kalman filter to assimilate real in situ data in a 1-d marine ecosystem
932 model.
- 933 Hoteit, I., G. Triantafyllou, and G. Petihakis (2005), Efficient data assimilation into
934 a complex, 3-d physical-biogeochemical model using partially-local kalman filters.
- 935 Huisman, J., P. van Oostveen, and F. J. Weissing (1999), Critical depth and criti-
936 cal turbulence: two different mechanisms for the development of phytoplankton
937 blooms, *Limnology and oceanography*, *44*(7), 1781–1787.

- 938 Ishizaka, J. (1990), Coupling of coastal zone color scanner data to a physical-
 939 biological model of the southeastern us continental shelf ecosystem: 2. an eulerian
 940 model, *Journal of Geophysical Research: Oceans*, *95*(C11), 20,183–20,199.
- 941 Jahnke, R. A. (2010), Global synthesis, in *Carbon and nutrient fluxes in continental*
 942 *margins*, pp. 597–615, Springer.
- 943 Johnson, K. (2016), The scientific rationale, design and implementation plan for a
 944 biogeochemical-argo float array, *Planning Group Rep.*
- 945 Johnson, K., and H. Claustre (2016), Bringing biogeochemistry into the argo age,
 946 *Eos*, *97*(10.1029).
- 947 Jones, E. M., M. E. Baird, M. Mongin, J. Parslow, J. Skerratt, J. Lovell, N. Margve-
 948 lashvili, R. J. Matear, K. Wild-Allen, B. Robson, et al. (2016), Use of remote-
 949 sensing reflectance to constrain a data assimilating marine biogeochemical model
 950 of the great barrier reef, *Biogeosciences*, *13*(23), 6441–6469.
- 951 Kalaroni, S., K. Tsiaras, G. Petihakis, I. Hoteit, A. Economou-Amilli, and G. Tri-
 952 antafyllou (2016), Data assimilation of depth-distributed satellite chlorophyll- α in
 953 two mediterranean contrasting sites, *Journal of Marine Systems*, *160*, 40–53.
- 954 Kay, S., R. McEwan, and D. Ford (2019), North west european shelf production
 955 centre northwestshelf_analysis_forecast_bio_004_011, quality information document,
 956 *Copernicus Marine Environment Monitoring Service.*
- 957 Key, R. M., A. Olsen, S. van Heuven, S. K. Lauvset, A. Velo, X. Lin, C. Schirnick,
 958 A. Kozyr, T. Tanhua, M. Hoppema, et al. (2015), Global ocean data analysis
 959 project, version 2 (glodapv2).
- 960 King, R. R., J. While, M. J. Martin, D. J. Lea, B. Lemieux-Dudon, J. Waters, and
 961 E. ODea (2018), Improving the initialisation of the met office operational shelf-
 962 seas model, *Ocean Modelling*, *130*, 1–14.
- 963 Lauvset, S. K., R. M. Key, A. Olsen, S. van Heuven, A. Velo, X. Lin, C. Schirnick,
 964 A. Kozyr, T. Tanhua, M. Hoppema, et al. (2016), A new global interior ocean
 965 mapped climatology: The 1×1 glodap version 2, *Earth System Science Data*, *8*,
 966 325–340.
- 967 Legge, O., M. Johnson, N. Hicks, T. Jickells, M. Diesing, J. Aldridge, J. Andrews,
 968 Y. Artioli, D. C. Bakker, M. T. Burrows, et al. (2020), Carbon on the northwest
 969 european shelf: Contemporary budget and future influences, *Frontiers in Marine*
 970 *Science*, *7*, 143.
- 971 Lellouche, J.-M., O. Le Galloudec, M. Drévilion, C. Régnier, E. Greiner, G. Gar-
 972 ric, N. Ferry, C. Desportes, C.-E. Testut, C. Bricaud, et al. (2013), Evaluation of
 973 global monitoring and forecasting systems at mercator océan, *Ocean Science*, *9*(1),
 974 57.
- 975 Lenartz, F., C. Raick, K. Soetaert, and M. Grégoire (2007), Application of an en-
 976 semble kalman filter to a 1-d coupled hydrodynamic-ecosystem model of the lig-
 977 urian sea, *Journal of Marine Systems*, *68*(3-4), 327–348.
- 978 Lengaigne, M., C. Menkes, O. Aumont, T. Gorgues, L. Bopp, J.-M. André, and
 979 G. Madec (2007), Influence of the oceanic biology on the tropical pacific climate in
 980 a coupled general circulation model, *Climate Dynamics*, *28*(5), 503–516.
- 981 Lenhart, H.-J., D. K. Mills, H. Baretta-Bekker, S. M. Van Leeuwen, J. Van
 982 Der Molen, J. W. Baretta, M. Blaas, X. Desmit, W. Kühn, G. Lacroix, et al.
 983 (2010), Predicting the consequences of nutrient reduction on the eutrophication
 984 status of the north sea, *Journal of Marine Systems*, *81*(1-2), 148–170.
- 985 Lutz, M. J., K. Caldeira, R. B. Dunbar, and M. J. Behrenfeld (2007), Seasonal
 986 rhythms of net primary production and particulate organic carbon flux to depth
 987 describe the efficiency of biological pump in the global ocean, *Journal of Geophys-
 988 ical Research: Oceans*, *112*(C10).
- 989 Madec, G., et al. (2015), Nemo ocean engine.
- 990 Mattern, J. P., C. A. Edwards, and A. M. Moore (2018), Improving variational data
 991 assimilation through background and observation error adjustments, *Monthly*

- 992 *Weather Review*, 146(2), 485–501.
- 993 Mirouze, I., and A. Weaver (2010), Representation of correlation functions in variational assimilation using an implicit diffusion operator, *Quarterly Journal of the*
- 994 *Royal Meteorological Society*, 136(651), 1421–1443.
- 995
- 996 Mogensen, K., M. Balmaseda, A. Weaver, M. Martin, and A. Vidard (2009),
- 997 Nemovar: A variational data assimilation system for the nemo ocean model,
- 998 *ECMWF newsletter*, 120, 17–22.
- 999 Mogensen, K., M. A. Balmaseda, A. Weaver, et al. (2012), The nemovar ocean data
- 1000 assimilation system as implemented in the ecmwf ocean analysis for system 4.
- 1001 Natvik, L.-J., and G. Evensen (2003), Assimilation of ocean colour data into a
- 1002 biochemical model of the north atlantic: Part 1. data assimilation experiments,
- 1003 *Journal of Marine Systems*, 40, 127–153.
- 1004 Nerger, L., and W. W. Gregg (2007), Assimilation of seawifs data into a global
- 1005 ocean-biogeochemical model using a local seik filter, *Journal of Marine Systems*,
- 1006 68(1-2), 237–254.
- 1007 Nerger, L., and W. W. Gregg (2008), Improving assimilation of seawifs data by the
- 1008 application of bias correction with a local seik filter, *Journal of marine systems*,
- 1009 73(1-2), 87–102.
- 1010 O’Dea, E., R. Furner, S. Wakelin, J. Siddorn, J. While, P. Sykes, R. King, J. Holt,
- 1011 and H. Hewitt (2017), The co5 configuration of the 7 km atlantic margin model:
- 1012 large-scale biases and sensitivity to forcing, physics options and vertical resolution,
- 1013 *Geoscientific Model Development*, 10(8), 2947.
- 1014 Oschlies, A., and V. Garçon (1999), An eddy-permitting coupled physical-biological
- 1015 model of the north atlantic: 1. sensitivity to advection numerics and mixed layer
- 1016 physics, *Global Biogeochemical Cycles*, 13(1), 135–160.
- 1017 Park, J.-Y., C. A. Stock, X. Yang, J. P. Dunne, A. Rosati, J. John, and S. Zhang
- 1018 (2018), Modeling global ocean biogeochemistry with physical data assimilation: a
- 1019 pragmatic solution to the equatorial instability, *Journal of Advances in Modeling*
- 1020 *Earth Systems*, 10(3), 891–906.
- 1021 Pauly, D., V. Christensen, S. Guénette, T. J. Pitcher, U. R. Sumaila, C. J. Walters,
- 1022 R. Watson, and D. Zeller (2002), Towards sustainability in world fisheries, *Nature*,
- 1023 418(6898), 689.
- 1024 Powley, H. R., J. Bruggeman, J. Hopkins, T. Smyth, and J. Blackford (2020), Sen-
- 1025 sitivity of shelf sea marine ecosystems to temporal resolution of meteorological
- 1026 forcing, *Journal of Geophysical Research: Oceans*, p. e2019JC015922.
- 1027 Pradhan, H. K., C. Völker, S. Losa, A. Bracher, and L. Nerger (2019), Assimilation
- 1028 of global total chlorophyll oc-cci data and its impact on individual phytoplankton
- 1029 fields, *Journal of Geophysical Research: Oceans*, 124(1), 470–490.
- 1030 Raghukumar, K., C. A. Edwards, N. L. Goebel, G. Broquet, M. Veneziani, A. M.
- 1031 Moore, and J. P. Zehr (2015), Impact of assimilating physical oceanographic data
- 1032 on modeled ecosystem dynamics in the california current system, *Progress in*
- 1033 *Oceanography*, 138, 546–558.
- 1034 Sathyendranath, S., R. J. Brewin, C. Brockmann, V. Brotas, B. Calton, A. Chuprin,
- 1035 P. Cipollini, A. B. Couto, J. Dingle, R. Doerffer, et al. (2019), An ocean-colour
- 1036 time series for use in climate studies: The experience of the ocean-colour climate
- 1037 change initiative (oc-cci), *Sensors*, 19(19), 4285.
- 1038 Shulman, I., S. Frolov, S. Anderson, B. Penta, R. Gould, P. Sakalaukus, and S. Lad-
- 1039 ner (2013), Impact of bio-optical data assimilation on short-term coupled physical,
- 1040 bio-optical model predictions, *Journal of Geophysical Research: Oceans*, 118(4),
- 1041 2215–2230.
- 1042 Siddorn, J., and R. Furner (2013), An analytical stretching function that combines
- 1043 the best attributes of geopotential and terrain-following vertical coordinates,
- 1044 *Ocean Modelling*, 66, 1–13.

- 1045 Skákala, J., D. Ford, R. J. Brewin, R. McEwan, S. Kay, B. Taylor, L. de Mora,
1046 and S. Ciavatta (2018), The assimilation of phytoplankton functional types for
1047 operational forecasting in the northwest european shelf, *Journal of Geophysical*
1048 *Research: Oceans*, 123(8), 5230–5247.
- 1049 Skákala, J., J. Bruggeman, R. J. Brewin, D. A. Ford, and S. Ciavatta (2020), Im-
1050 proved representation of underwater light field and its impact on ecosystem dy-
1051 namics: a study in the north sea, *Journal of Geophysical Research: Oceans*, p.
1052 e2020JC016122.
- 1053 Smyth, T. J., I. Allen, A. Atkinson, J. T. Bruun, R. A. Harmer, R. D. Pingree,
1054 C. E. Widdicombe, and P. J. Somerfield (2014), Ocean net heat flux influences
1055 seasonal to interannual patterns of plankton abundance, *PloS one*, 9(6).
- 1056 Song, H., C. A. Edwards, A. M. Moore, and J. Fiechter (2016), Data assimilation in
1057 a coupled physical-biogeochemical model of the california current system using an
1058 incremental lognormal 4-dimensional variational approach: Part 3assimilation in
1059 a realistic context using satellite and in situ observations, *Ocean Modelling*, 106,
1060 159–172.
- 1061 Storkey, D., E. Blockley, R. Furner, C. Guiavarch, D. Lea, M. Martin, R. Barciela,
1062 A. Hines, P. Hyder, and J. Siddorn (2010), Forecasting the ocean state using
1063 nemo: The new foam system, *Journal of operational oceanography*, 3(1), 3–15.
- 1064 Swart, S., S. J. Thomalla, and P. Monteiro (2015), The seasonal cycle of mixed layer
1065 dynamics and phytoplankton biomass in the sub-antarctic zone: A high-resolution
1066 glider experiment, *Journal of Marine Systems*, 147, 103–115.
- 1067 Telszewski, M., A. Palacz, and A. Fischer (2018), Biogeochemical in situ
1068 observations—motivation, status, and new frontiers, *New Frontiers in Operational*
1069 *Oceanography*, pp. 131–160.
- 1070 Torres, R., J. Allen, and F. Figueiras (2006), Sequential data assimilation in an
1071 upwelling influenced estuary, *Journal of Marine Systems*, 60(3-4), 317–329.
- 1072 Triantafyllou, G., G. Korres, I. Hoteit, G. Petihakis, and A. Banks (2007), As-
1073 similation of ocean colour data into a biogeochemical flux model of the eastern
1074 mediterranean sea.
- 1075 Vaquer-Sunyer, R., and C. M. Duarte (2008), Thresholds of hypoxia for marine
1076 biodiversity, *Proceedings of the National Academy of Sciences*, 105(40), 15,452–
1077 15,457.
- 1078 Verdy, A., and M. Mazloff (2017), A data assimilating model for estimating s out-
1079 hern o cean biogeochemistry, *Journal of Geophysical Research: Oceans*, 122(9),
1080 6968–6988.
- 1081 Visbeck, M., M. Araujo, A. Boetius, E. Buch, H. Claustre, T. Dabrowski, E. Delory,
1082 B. de Young, K. Drinkwater, A. Fischer, et al. (2015), More integrated and more
1083 sustainable atlantic ocean observing (atlantos), *CLIVAR Exchanges*, 67(2), 18–20.
- 1084 Waniek, J. J. (2003), The role of physical forcing in initiation of spring blooms in
1085 the northeast atlantic, *Journal of Marine Systems*, 39(1-2), 57–82.
- 1086 Waters, J., D. J. Lea, M. J. Martin, I. Mirouze, A. Weaver, and J. While (2015),
1087 Implementing a variational data assimilation system in an operational 1/4 de-
1088 gree global ocean model, *Quarterly Journal of the Royal Meteorological Society*,
1089 141(687), 333–349.
- 1090 While, J., K. Haines, and G. Smith (2010), A nutrient increment method for re-
1091 ducing bias in global biogeochemical models, *Journal of Geophysical Research:*
1092 *Oceans*, 115(C10).
- 1093 Xing, X., H. Claustre, S. Blain, F. d’Ortenzio, D. Antoine, J. Ras, and C. Guinet
1094 (2012), Quenching correction for in vivo chlorophyll fluorescence acquired by
1095 autonomous platforms: A case study with instrumented elephant seals in the ker-
1096 guelen region (southern ocean), *Limnology and Oceanography: Methods*, 10(7),
1097 483–495.

1098 Yu, L., K. Fennel, L. Bertino, M. El Gharanti, and K. R. Thompson (2018), In-
1099 sights on multivariate updates of physical and biogeochemical ocean variables
1100 using an ensemble kalman filter and an idealized model of upwelling, *Ocean Mod-*
1101 *elling*, 126, 13–28.

Accepted Article